Energy Storage Materials 69 (2024) 103413

Contents lists available at ScienceDirect

Energy Storage Materials

journal homepage: www.elsevier.com/locate/ensm

Impedance spectroscopy applied to lithium battery materials: Good practices in measurements and analyses

Sara Drvarič Talian [a], Sergio Brutti [b,c], Maria Assunta Navarra [b,c], Jože Moškon [a], Miran Gaberscek [a,d,*]

[a] ALISTORE European Research Institute (ALISTORE ERI) - Department of Materials Chemistry, National Institute of Chemistry, Hajdrihova 19, Ljubljana, 1000, Slovenia
[b] ALISTORE European Research Institute (ALISTORE ERI) - Dipartimento di Chimica, Università di Roma La Sapienza, P.le Aldo Moro 5, 00185 Roma, Italia
[c] GISEL-Centro di Riferimento Nazionale per i Sistemi di Accumulo Elettrochimico di Energia, 50121, Florence, Italy
[d] Faculty of Chemistry and Chemical Technology University of Ljubljana, Večna pot 113, Ljubljana, 1000, Slovenia

ARTICLE INFO

Keywords:
Electrochemical impedance spectroscopy
Aprotic batteries
Equivalent circuit
Continuum level modeling
Impedance transmission line

ABSTRACT

This paper outlines a critical analysis of the currently available methodological framework for a comprehensive and reliable interpretation of impedance spectroscopy data of aprotic lithium-based secondary batteries. Impedance spectroscopy is a powerful experimental technique that can be used to assess the impedance of batteries over a range of frequencies. However, in typical battery configurations, all components contribute to the impedance response of the whole cell and the overlap of many of the different impedance responses often results in a complex experimental curve that is not easily easy to interpret. Various analytical approaches can be used to evaluate complex impedance data sets of batteries: (a) matching the impedance response of the cells in question with a previously published impedance model; (b) performing additional electrochemical measurements with different settings and/or on different cell designs to support the assignation of impedance contributions to specific physicochemical processes; (c) acquiring external physicochemical determinations, morphological and chemical data that can support or refute the results of impedance analysis; (d) developing theoretical models that reconcile physical insights at different length scales of the battery components with the equivalent circuit formalism.

1. Introduction

Electrochemical impedance spectroscopy (EIS) is an experimental technique that can evaluate the impedance of a dielectric system, either redox or capacitive, over a range of frequencies [1–3]. Experimentally an EIS experiment is realized by applying an electric stimulus (e.g. a known voltage or current oscillation with known frequency) to an electrochemical cell constituted at least by two electrodes separated by a dielectric layer. The output electrical signal is recorded, elaborated and the outcome data expressed numerically and graphically (e.g. the so-called Bode or Nyquist plots) [3]. The general assumption of impedance spectroscopy experiments is that physico-chemical properties of the electrochemical cell are time-invariant, and the overall cell is unaltered at the end of the EIS experiment compared to the pristine state [1,2]. Thus, multiple consecutive EIS experiments are expected to give identical results. Starting from the late 70 s, Automated data acquisition systems become available for fast processing of the large data flow produced in an EIS experiment [4,5]. Overall, the introduction of automatic numerical elaboration systems boosted the exploitation of this electrochemical technique as proved by the innumerable published papers reporting EIS data.

There are various possible technical alternatives to implement an EIS experiment: the most common and typical approach, is to measure impedance by applying a series of single-frequency voltage signals to the working electrode of a three or two electrode cell and measuring the phase shift and amplitude of the resulting current at that frequency. Commercial instruments can handle frequency signals from below 0.1 mHz to 1 MHz and are operated by automated graphical interfaces to facilitates the realization of experiments. The subsequent elaboration of EIS primary data (frequency, phase shift, amplitude) can disclose physico-chemical properties of any electrochemical systems and its constituents, in particular:

* Corresponding author.
E-mail address: miran.gaberscek@ki.si (M. Gaberscek).

https://doi.org/10.1016/j.ensm.2024.103413
Received 1 February 2024; Received in revised form 12 April 2024; Accepted 16 April 2024
Available online 23 April 2024

List of symbols

C_{chem}	chemical capacitance
C_{dl}	double layer capacity
$c^0_{M^{z+}}$	concentration of active ion M^{z+}
c_{salt}	molar concentration of salt dissolved into the electrolyte
D_{chem}	chemical diffusional coefficient
$D_{chem,eff}$	effective chemical diffusional coefficient
$D_{M^{z+}}$	diffusion coefficient of active ion M^{z+} reacting with parent electrode M
E_a	activation energy
f	frequency
F	Faraday's constant
i	Imaginary unit
$I(\omega)$	current response to sinusoidal excitation
$I_{0,\omega}$	maximum value of the sinusoidal response current to voltage excitation
k^0_b	potential independent rate constant parameter for reduction
K	dielectric constant of the electrolyte
L	thickness of the electrolyte layer
L_D	effective thickness of the double layer region
L_p	thickness of porous electrode
N_M	MacMullin number
R	gas constant
R_{ct}	charge transfer reaction resistance
R_{el}	the resistance of the electrolyte layer
S	geometrical surface area of electrodes
T	temperature
$V(\omega)$	alternate small voltage bias
V_0	is the maximum value of the alternating voltage bias
z	valence number of transported active ion
Z_{im}	imaginary portion of the complex impedance
Z_{real}	real portion of the complex impedance
$\|Z\|$	modulus of the impedance of system under consideration
Z_W	Warburg impedance
α	Bruggerman exponent
ε	porosity
ε_0	permittivity of vacuum
κ	conductivity of the electrolyte
Λ^o_{total}	total molar conductivity
τ	relaxation time
τ_g	tortuosity
φ	phase shift
ω	angular frequency

1. properties of the electrode/electrolyte materials (e.g. conductivity, dielectric constants, charge mobilities, equilibrium concentration of the ions)
2. properties of the electrode/electrolyte interface (e.g. time constants, kinetic rate constants and capacitance)

In this work we tackle a rational evaluation of the current methodological approaches exploited in the scientific literature in the application of EIS to lithium aprotic secondary batteries (ASB). In this respect we aim to provide a critical assessment of the most crucial aspects to implement a reliable and informative EIS experiment ranging from its experimental implementation to the dataset analysis and interpretation. Starting from this general introduction (Section 1), the structure of this work follows this rationale sequence: in the Section 2 some EIS fundamental quantities and concepts are outlined, in Section 3 we explain the available modeling approaches and in Section 4 we review good literature practices and connect the various approaches to cell components.

2. Impedance spectroscopy: definitions and fundamental quantities

All galvanic electrochemical cells, either primary or secondary, are constituted by multiple components that contribute to the impedance response of the whole cell. Focusing on ASBs, a general schematization is shown in the Fig. 1.

It is possible to identify seven different constituent elements unavoidably present in all ASBs formulations, which can be grouped in four categories depending on the time constant of their main impedance response to an alternating voltage bias:

1. The positive and the negative metallic current collectors
2. The electrolyte-soaked separator.
3. The electrode/electrolyte interphases at the negative and positive sides
4. The positive and the negative composite electrodes

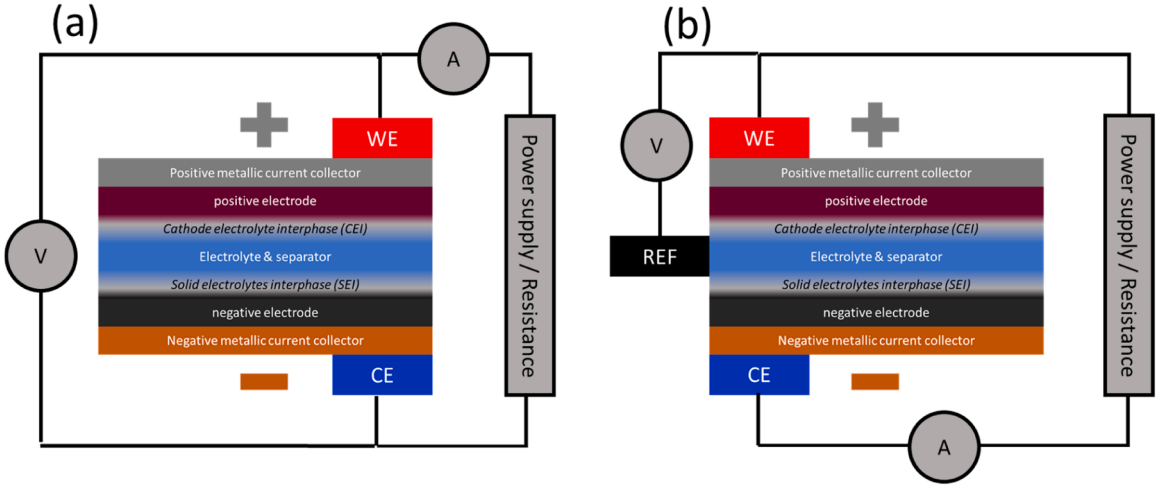

Fig. 1. Electrochemical cells for EIS in (a) two and (b) three electrodes' configurations. WE = working electrode, CE= counter electrode; REF= reference electrode, A = amperemeter; V = voltmeter.

All these seven components of ASBs contribute to the impedance response to a different extent and in different frequency ranges. Thus, the resulting experimental outcome of any EIS experiment is a complex overlap of contribution originated from various components of the cell. Consequently, despite the ability of EIS to discriminate electrochemical phenomena predominant at different frequencies, the complexity of the electrochemical cell shown in the Fig. 1 unavoidably makes the interpretation of impedance outcomes very hard. Thus, there is a need for a robust interpretation model or methodology to fully disclose all the information integrated within the EIS experimental trace [6].

From the experimental point of view, EIS experiments can be carried out in two different cell configurations as shown in the Fig. 1: (a) two electrodes configuration; (b) three electrodes configuration. In the two electrodes configuration the alternating voltage bias is applied at the working electrode (WE) in respect to the counter electrode (CE) and the response current is measured between the WE and the power supply/external resistance. Therefore, the alternating voltage bias stimulates the impedance response from all the seven components of the cell. This configuration is mandatory to evaluate the overall impedance response of the whole cell, as an example in the case of state-of-health evaluations of batteries. In the three electrodes configuration the alternating voltage bias is applied at the working electrode (WE) in respect to an ideal non-polarizable reference electrode (REF, i.e. an ideal electrode in which a faradic current can freely pass and its potential does not change from its equilibrium one upon application of current) and the response current is measured between the power supply/external resistance and the CE. Consequently, the alternating voltage bias limits the impedance response only from the WE-end of the cell (e.g. positive metallic current collector/composite positive electrode/cathode electrolyte interphase/electrolyte & separator). This configuration is mandatory to facilitate the decoupling of the impedance contribution originating from the WE, the interphase, and the electrolyte. Furthermore, the use of redox-inactive WE and CE (the so-called blocking electrodes), either in the two or three electrode configurations, allows to focus on the sole impedance response of the electrolyte/separator, being the role of both positive and negative electrode/electrolyte ends purely capacitive.

Overall, EIS experiments in two electrodes configurations are always technically feasible despite unavoidable overlap between the impedance response of the WE and CE. This configuration allows to easily monitor the aging of a single cell, but the decoupling of the contributions originated from the different cell components is challenging. On the other hand, three electrodes' configurations limit the complexity of the impedance response and allow focus on the WE-end part of the cell. Unfortunately, three electrodes' configurations are not always technically feasible, especially in commercial batteries. In R&D laboratories EIS experiments can be designed and realized in controlled conditions and therefore the experimental setup can be selected based on the research goal.

Before continuing it is important to discuss the main sources of experimental errors in EIS experiments in ASBs. As mentioned above, a reliable EIS experiments requires that the physico-chemical properties of the electrochemical cell are time-invariant, and the overall cell is unaltered at the end of the EIS experiment compared to the pristine state. This pre-requisite is often under-evaluated, leading to artifacts in the impedance response originating from transient states and not from well-equilibrated systems. Furthermore, it is important to underline that the frequency of the alternating voltage bias can vary in EIS by several order of magnitudes, ranging from megahertz to microhertz. In this respect EIS experiments can last hours, thus requiring careful control of additional experimental conditions such as the cell temperature. However, depending on the phenomena of interest, the relevant frequency ranges can be more limited but may possibly require careful choices of the experimental conditions (e.g. automatic current ranges, current pre-ranging, number of datapoints, voltage bias) and/or an accurate data averaging (multiple wave accumulation, relaxation times between frequencies, …).

In summary, to minimize the possible source of experimental errors, it is important to design appropriate experimental protocols considering both the need of well-equilibrated systems as well as well-planned experimental conditions.

1. Initially, one must scrutinize the parameters of the impedance measurements to ensure the desired physical-chemical processes are being measured and the spectra are reliable.
2. Non-trivially, several repetitions of measurements on the same cell and parallel measurements on identically prepared cells is needed to ensure relevant data is being measured. Another way to ensure that the cell is stable enough to measure its impedance spectra is by using a prerequisite equilibration period before EIS measurement. This is true for both EIS measurements at OCV or when EIS measurements are conducted during a voltage hold.
3. After ensuring that the spectra do not have interference from outside sources and that EIS measurements are repeatable, the adequate frequency range of the measurement should be optimized for the evaluation of a given process occurring in a given time-scale. Namely, if for very slow processes, their impedance features can be observed only by extending the measurement into the low frequency range.

In an EIS experiment for the investigation of ASBs, both in two or three electrodes' configurations, the most common and typical approach is to measure impedance by applying a series of single-frequency voltage signals to the working electrode of a three or two electrode cell and measuring the phase shift and amplitude of the resulting current at that frequency [6,7]. The time dependence of the applied alternate voltage bias $V(t)$ and the current response $I(t)$ are:

$$V(\omega) = V_0 \cdot e^{i\omega t}. \tag{E1}$$

$$I(\omega) = I_{0,\omega} \cdot e^{i(\omega t+\varphi)} \tag{E2}$$

Where V_0 is the maximum value of the alternating voltage bias for a given ω angular frequency (i.e. $\omega = 2\pi \cdot f$, where f is applied frequency of the voltage bias), $I_{0,\omega}$ is the resulting maximum value of the response current at ω and φ is the phase shift of the current response. For a given ω, the impedance response of the cell is given by:

$$Z(\omega) = \frac{V(\omega)}{I(\omega)} \tag{E3}$$

Simple algebraic manipulations allow to reformulate Eq. (E3) as follows:

$$Z(\omega) = Z_{real} + i \cdot Z_{im} \tag{E4}$$

Where Z_{real} and Z_{imm} and the real and the imaginary portions of the complex impedance at a given frequency, respectively. The resulting dataset for an EIS experiment is constituted by a series of triplets $(f; |Z|; \varphi)$ or $(f;\ Z_{real}; Z_{imm})$ that can be represented in the so called Bode-plot or Nyquist-plot as shown in the Fig. 2.

In the large part of the existing literature concerning the use of impedance spectroscopy in battery applications, only the Nyquist plot is used as a starting point for any further data analysis or interpretation: this approach is correct but incomplete. The two traces, which are both a convolution of signals originating from different phenomena, show the same experimental datasets and any fitting model must find a reasonable match in the most evident features of both representations.

The occurrence of a phase shift between the alternating voltage bias and the resulting alternating current origins depends on the impedance response of each component (e.g. resistive or capacitive) and interface (capacitive or faradic) of the ASB. As an example, purely resistive constituents (e.g. electrolytes) give a phase invariant impedance response, whereas pure capacitive elements (e.g. metallic electrode surfaces) give a 90° phase shift.

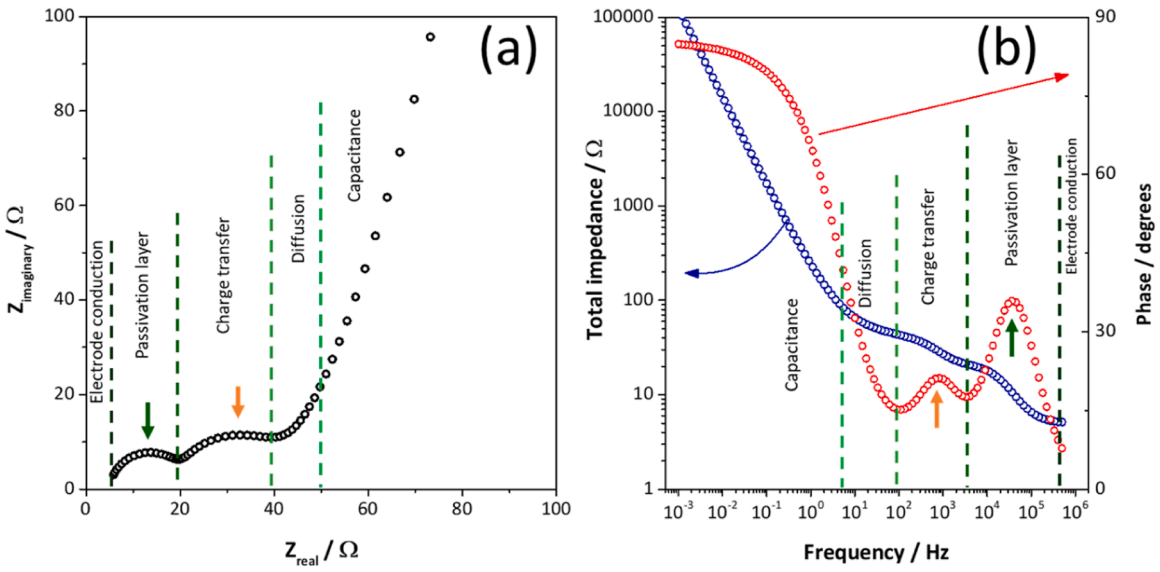

Fig. 2. Examples of the so called (a) Nyquist plot and (b) Bode plot. Kinetic steps common in most batteries and related simulated qualitative EIS spectra of an intercalation electrode.

The most typical feature of any EIS spectra in the Nyquist plot is the well-known semi-circular fingerprint of an active interface between two media with different homogenous dielectric properties. Any interface is constituted by a double layer of charges, which can be either capacitive or faradic. Within each double layer, the motion of charges occurs in a timescale that matches the frequency of the maximum of this semi-circular feature in the Nyquist plot, or the maximum of the phase in the corresponding Bode plot. As already discussed, from a technical point of view in any EIS experiment, it is possible to modulate the voltage frequencies applied to a battery in a broad range, from MHz to below mHz. This capability provides information about the impedance response of any battery system at various frequencies and allows decoupling of phenomena that involve the motion of charges at different timescales. Overall batteries are complex systems where charges move across all interfaces (see the Fig. 1) with specific time-constants that can vary by order of magnitudes, as shown qualitatively in the Fig. 2.

In this respect one may qualitatively consider that it is possible to decouple the various parallel charge motion processes considering the frequency range in which their impedance fingerprint is observed in any cell geometry/formulation like a standard coin cell:

1. Electron motions in electrodes, ion motions in the bulk of the electrolyte (resistive homogenous media): $f > 50$ kHz
2. Ion transport across a permeable passivation layer (capacitive double layer): $f \approx 0.1$–50 kHz
3. Charge transfer phenomena (faradic double layer): $f \approx 10$–1000 Hz
4. Diffusion in the solid state of ions involved in faradic process (so-called Warburg-diffusion): $f \approx 10$–100 mHz
5. Accumulation of charge of the electrode surface (capacitive double layer): $f \approx 0.01$ - 10 mHz

These ranges are qualitative and may easily overlay, especially in porous electrodes or in all cases in which a complex parasitic chemistry occurs. However, any qualitative analysis of an EIS spectra resulting from the investigation of a lithium battery electrode, requires taking into consideration these timescales and the corresponding sequence of phenomena. In this respect the qualitative observation of the impedance trace represented using either the Bode or the Nyquist plots allow to draw the sequence of phenomena that contributes to the EIS response of the cell and the corresponding frequency ranges. This preliminary qualitative analysis is mandatory for any further modelling or deconvolution approach to avoid over-interpretation of the EIS dataset [8].

The overlap of many of the various impedance responses of the ASB components often leads to a complex experimental curve not easily understandable without modelling efforts. However, some qualitative analyses are possible based on the direct observation of the EIS data using either the Bode or the Nyquist representations. In all cases where semi-circular features (i.e. arcs) are observed in the Nyquist plot in different frequency ranges. The evolution of the arc shape and dimensions can be clue of different phenomena:

- The effect of electrolyte conductivity and separator properties shift the intercept with the real impedance axis of the high frequency semi-circle in the Nyquist plot (see Fig. 3a). In the example shown, the spectral features of the high frequency semi-circle remain constant (i.e. frequency and Z_{real} of the maxima of the semicircle) while the resistance of electrolyte increases. This kind of trend in the EIS trace is a direct qualitative fingerprint of an active degradation chemistry that involves the electrolyte/separator component of the ASB.
- The increase in the size of the semi-circular diameter is a clue of an increase in the resistive character of the impedance response (see Fig. 3b). This spectral change goes typically in parallel with the decrease of the frequency corresponding to the maximum of the semi-circular feature. The increase in the resistive character of an interface can originate in the case of a passivation layer, either from its thickening or composition evolution that enrich insulating constituents, and in the case of a charge transfer from the increase in the kinetic hinderance of the process, promoted by smaller reagent activities.
- The stable size of the semi-circular diameter occurring in parallel to the downward shift of the frequency of the maximum is direct evidence of an increase of the capacitive character of the impedance response (see Fig. 3c). The increase in the capacitive response of an interface can derive from an increase in the electrochemical active surface of the double layer, either in the case of a passivation film or in the case of a charge transfer phenomena.

Typically, these changes occur simultaneously, thus making impossible a qualitative decoupling of the physico-chemical effects that are driving the alteration of the EIS response. This evidence shows a clear need for modeling the impedance response of ASB by computational

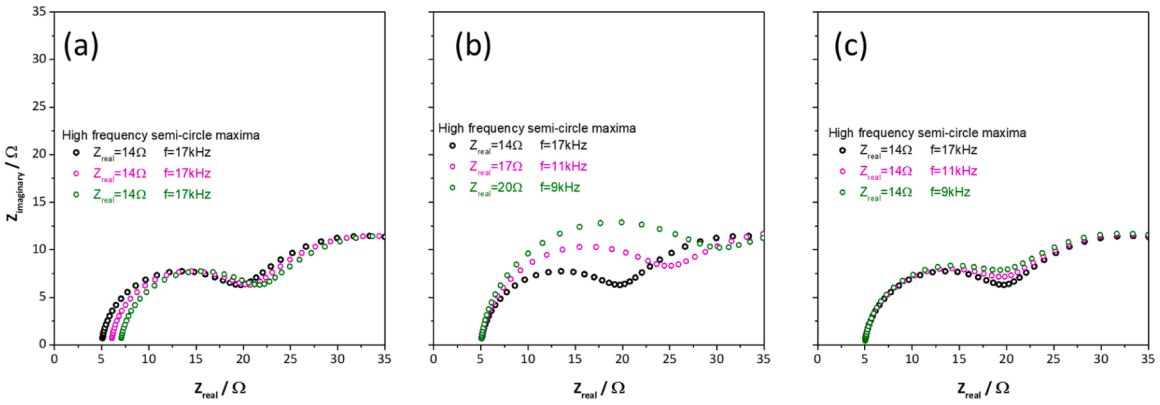

Fig. 3. Examples of simulated EIS spectra.

methods based on the so-called equivalent circuit approach or more complex physically funded approaches.

Recently, an alternative approach of data representation has been gaining momentum: the so-called distribution of relaxation times concept [9–11]. This approach is based on a transformation of the experimental data from the frequency domain to a distribution function of relaxation times (DRT or DFRT). In principle such a transformation can led to a better separation, in particularly better visualization, of the underlying electrochemical processes which are seen as peaks with characteristic time constants that are associated with the separate processes, e.g. Fig. 4.

3. Analysis of EIS applied to ASB: approaches to experiments and modelling

To provide a concise overview of the different possibilities of applying EIS to battery research, here we outline and discuss the experimental approaches from the simplest towards more complex. In the next chapter, these approaches are linked to cell components and processes, providing an outline of which concept is most suitable for an analysis of a given cell phenomenon. With this we aimed to showcase good practices available in the literature, explaining the methodology and analyses behind it.

3.1. *Approach 1: measuring basic impedance response of studied systems and fitting by applying an arbitrary simple single-rail model*

The simplest approach to employing impedance spectroscopy to study battery systems is to match the impedance response of cells in interest with an already published impedance model. This is a common method in the literature and is frequently employed in studies where impedance spectroscopy is an auxiliary technique used to support hypothesis grounded on other electrochemical or chemical characterization techniques.

With this approach, several requirements need to be met for the results to be reliable. First, dedicated impedance spectroscopy studies -

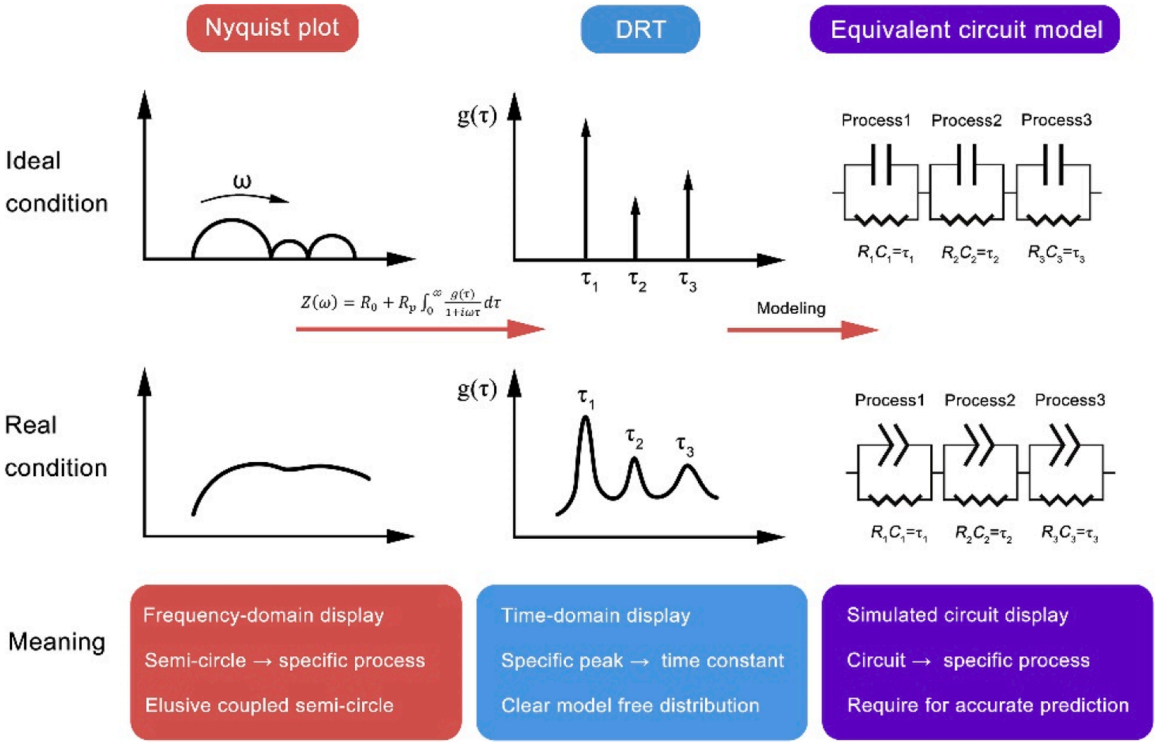

Fig. 4. Example of a transformation of the experimental data from the frequency domain to a distribution function of relaxation times (DRT or DFRT) obtained from ref. [10].

where impedance-sensitive parameters are well controlled - rather than routine measurements should be the basis of the employed model. Secondly, a published model is only applicable if the system under consideration is identical or at least similar to the published one. Finally, the use of equivalent circuit models should be conducted with care. To explain this, simple single-rail equivalent circuit models are often chosen according to the shape of the impedance spectrum in the Nyquist plot representation and assume that one major impedance feature (e.g. impedance arc) corresponds to a single electrochemical process. For example, if the arc is depressed, the inconsistencies are masked through using a constant phase element instead of an ideal capacitor for the capacitive component. This simple assumption of "one arc – one process" does not apply to complex electrochemical systems and can lead to incorrect explanations of impedance spectra, which can be the cause of dubious literature reports. Furthermore, the same impedance spectrum can be (approximately or in some cases even exactly) simulated with multiple different circuits. Use of simple single-rail equivalent circuit models is therefore suitable only in model battery cell systems, where one can be sure that each impedance arc/feature is due to a single transport or electrochemical process and for which we have good comprehension about the impedance contributions' origins.

3.2. Approach 2: additional impedance measurements and analyses

A first level of added complexity with an original impedance spectroscopy study is to conduct additional electrochemical measurements with different settings and/or on different cell designs to support the assignation of impedance contributions to specific physical-chemical processes.

For cells with asymmetric electrodes type cells (full cells), additional impedance spectra measurements must be first carried out to separate electrode contributions between cathode and anode. There are two common ways of dealing with this problem: Measuring the spectra of three-electrode cells or building symmetric cathode-cathode and anode-anode cells. The first option, using a three-electrode cell, means building a special cell that contains an additional reference electrode. This electrode allows for measurements of spectra specific to the positive or the negative electrode. Furthermore, it also allows for in situ measurements and changing the cell state of charge (SOC) between impedance spectra determinations. The problem with reference electrodes is that it is difficult to design a stable and reliable one. A reference electrode must not interfere with the reactions taking place on the anode or the cathode and be small enough to not disturb the electric field between them. It also must have a stable potential. If these requirements are not met, the measurements can be subject of considerable errors. These can manifest as middle frequency loops [12] or even hidden features that are sometimes difficult to detect. There are only few reports on the use of stable reference electrodes in battery cell research [13,14], that provide reliable impedance spectra measurements.

The second option in differentiating between cathode and anode contributions is building symmetric cells out of full cell parts [15–17]. This means that two close-to identical full cells need to be assembled and treated equally before their impedance spectra are measured. These cells are then disassembled and out of the available cell parts, two symmetric cells are made, and their impedance spectra are measured. This method circumvents the issues with building more technically demanding three-electrode cells and the problems associated with finding stable and reliable reference electrodes. Although not in situ, change in SOC or other parameters can still be achieved. Nevertheless, precautions associated with potential cell change during disassembly, such as electrolyte dry out, need to be considered and properly assured.

Apart from using reference electrodes and the symmetric cell approach, there are other tricks which might be handy in differentiating between cathode and anode impedance contributions. An example is drastically increasing the surface area of the electrode, which is not the focus point of the study (the counter electrode). This reduces its impedance contributions and, ideally, makes them negligible. What is left on the impedance spectrum is the working electrode impedance contributions. This can be further improved by additionally reducing the size of the working electrode. When manipulating the electrode sizes, the overall design of the cell must be carefully considered. In such cases one usually must resort to a flooded cell type rather than using the separator type cells that are commonly used in battery research. This is due to the fact that when using a thin separator, the electrodes are close to each other. The electric field going from the smaller working electrode therefore might not encompass the full desired surface area of the large counter electrode, significantly reducing the active portion of the counter electrode and not reaching the desired effect.

After separating positive and negative electrode contributions, the next step is an attempt to simplify the cell design, which hopefully leads to a more straightforward impedance spectrum. In this part of the approach, the idea is to get rid of complex or overlapping impedance arcs. This would hopefully lead to a quite simple spectrum, where fitting with equivalent circuit models is desirable and does not usually produce significant errors, since impedance arcs are ideally resolved and correspond to a single physical-chemical process. From there, the excluded complications are systematically added back into cell design to reach the starting point but with more in-depth knowledge on the origin of impedance contributions.

Besides simplification, several other cell design changes can be immensely helpful in accurate impedance spectra analysis. The first one is changing the concentration of supporting salt in the electrolyte. This is usually done by the orders of magnitude (e.g. 1 M, 0.1 M, 0.01 M or even lower) [18,19], to ensure that change is sufficiently visible. If we decrease the supporting salt concentration, several impedance contributions change in a predictable way. At this point, let us note that changing the concentration may also affect the activity coefficient, so one needs to adjust the analysis if change in activity coefficient is relevant.

The charge transfer reaction resistance R_{ct} is inversely dependent on the active species concentration. In simplified terms, this means that reducing the concentration of the active species will proportionally increase the resistance due to the species' charge transfer reaction. This is shown as an increase of the size of the arc marked with green on Fig. 5. This is of course true if the species, whose concentration was changed, enters the redox reaction from the solvated state. If the species first adsorbs on the electrode surface, then a change in the surface specific concentration needs to happen to vary the R_{ct} value [20]. Similarly, the charge transfer reaction might be happening at the interface between a compact passive layer and the bulk electrode, in which case the concentration of the species inside the compact layer is the relevant one.

Apart from changing the concentration of charge-carrier species, electrolyte dilution also changes its viscosity. Both of those mean that the conductivity of the electrolyte will also change, although the correlation is not strictly straightforward. Namely, when increasing the concentration of charge-carrier species in the electrolyte solvent, the conductivity increases until we reach a point that their mobility becomes an issue due to high electrolyte viscosity. At that point, the conductivity plateaus and starts decreasing if more salt is added [21]. Battery electrolytes are usually prepared to be at the maximum conductivity value, so the most likely scenario is that reducing the electrolyte concentration will decrease both its viscosity as its conductivity. This will be evident in the impedance spectra as an increase in the resistive intercept - all EIS spectra of well-behaving aprotic lithium-based batteries almost intercepts the real impedance axis at its highest frequency, typically at 1 MHz-50 kHz (see the Nyquist plots in Figs. 2 and 3). This real impedance value reflects transport phenomena through a homogeneous media of a highly mobile charge carrier, i.e. all ions solvated in the electrolyte, and is commonly denoted as the electrolyte resistance (R_{el}). The R_{el} value measured by EIS is closely related to physical chemical properties of the electrolyte [8]:

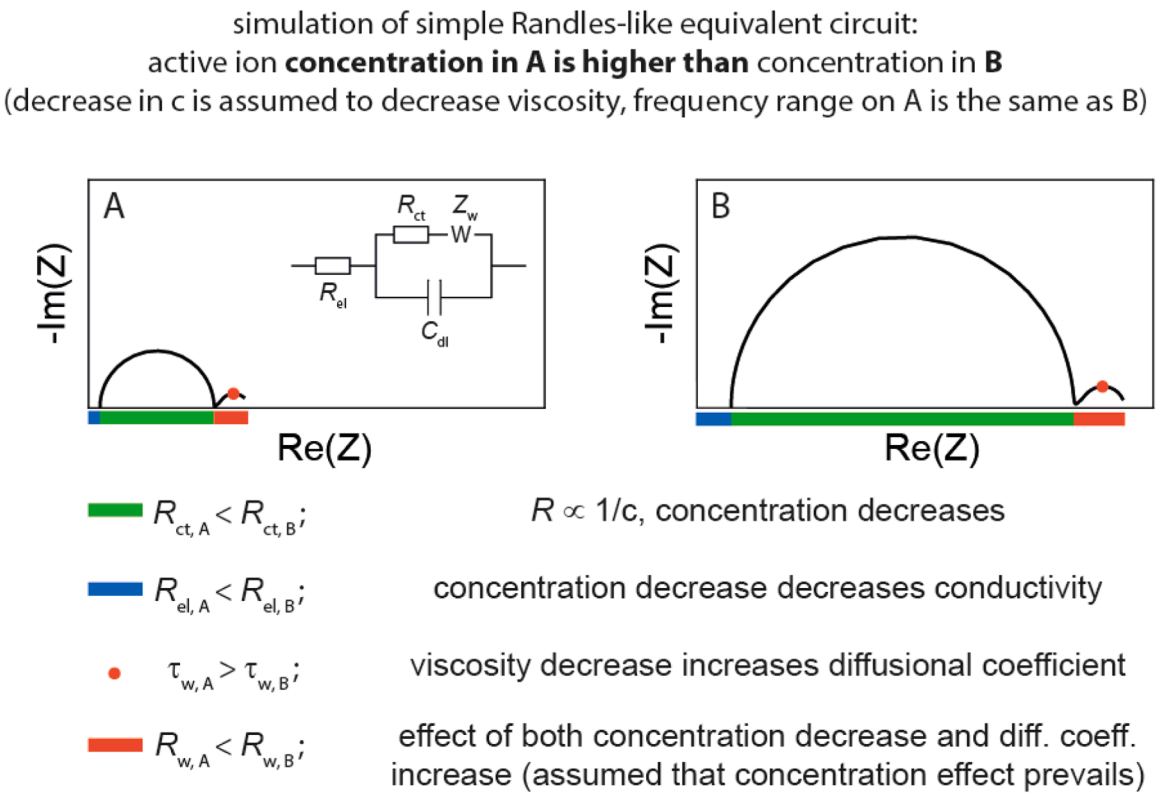

Fig. 5. Example of simulation of simple impedance spectrum and the change induced due to a decrease in electrolyte concentration.

$$R_{el} = \frac{N_M}{\kappa}\frac{L}{S} \quad \text{(E5)}$$

Where κ is the conductivity of the electrolyte (in S m^{-1}), L is the thickness of the electrolyte layer (in m, i.e. the linear distance from the working electrode to the counter electrode), S is the surface of electrodes (in m^2) and N_M is the MacMullin number (dimensionless, $N_M > 0$ where $N_M = 1$ in the case of a pure isotropic liquid with no relevant steric constraints that hinders the motion of ions from the bulk to the electrode surface) [22]. Generally speaking the N_M can be derived from the tortuosity τ_g and the porosity ε of the conductive media by the $N_M = \tau_g / \varepsilon$ equation, being these two last dimensionless quantities related through the empirical Bruggerman relation $\tau_g = \varepsilon^{\alpha}$, where α is the Bruggerman exponent [23,24].

Viscosity change also affects the value of the chemical diffusional coefficient (decrease in viscosity increases D_{chem}). Due to both diffusion coefficient and concentration change, the Warburg arc resistance size will differ (Fig. 5). It will also shift to different characteristic frequencies - in the case of viscosity decrease, the time constant for the diffusional contributions will decrease and the peak frequency increase. Electrolyte concentration change therefore changes multiple parameters defining the impedance spectra size and shape. It is important to note that although these specific impedance contributions will change, it is also possible the impedance spectrum will not significantly change overall. This is especially true for cells with a complex mix of low-frequency diffusion process (such as solid-state diffusion in Li-ion cells), where the diffusional contributions due to electrolyte filled porous layers are hidden behind larger solid-state diffusion impedance.

Besides changing the electrolyte concentration, a simple manipulation is changing the thickness of the porous layers in the cell through which diffusional processes take place. This part of the approach, for example, encompasses preparation of electrodes of different thicknesses [25,26], changing the thickness of artificially prepared coatings or layers and stacking multiple separators on top of each other [27]. We suggest a change of at least a factor of 3 to be sure of the impact on the impedance contributions. Of course, even more information is gathered if the thickness is changed in several steps – L_p, 3 L_p, 9 L_p. Changing the thickness parameter of electrochemically inactive components (stable artificial porous layers, separator) will influence the transport processes taking place in this part of the cell. A change in the porous electrode material thickness, on the other hand, will also influence the reactional contributions. This is because keeping the porosity and tortuosity constant necessitates a surface area increase.

Specifically explaining the expected differences when varying thicknesses of non-conductive cell layers, changing the thickness has an influence on the value of the resistive intercept and the Warburg resistance due to diffusion through this specific non-conductive porous layer. The manipulation also affects the capacitive contribution and the time constant for the layer's diffusion contribution. Note that the difference in the spectrum might be negligible in the case of small overall separation change. In the high frequency part of the spectra, where we expect the migration contributions of electrolyte filled non-conductive layers, common battery research laboratory impedance spectroscopy measurement instruments do not have the capability of resolving the different contributions.

As mentioned, the thickness change in the conductive electrode layer part of the cell induces more complex shifts in the impedance spectrum. The reaction contribution depends on the electrode active surface area. If we increase the thickness of the electrode with keeping other parameters identical (porosity, particle size, etc.), then the charge transfer resistance will decrease due to larger available electrode surface area. The peak frequency, on the other hand should remain identical, since the double layer capacitance of the electrode will increase through a reverse relation to the available surface area. Secondly, the transport through the electrode will change due to longer paths the species have to/can travel. These changes happen in both the low and high frequency parts of the spectra. The impedance contribution due to migration of species in the porous electrode is usually separated from the migration contributions in non-active layers (which are included in the high frequency

resistive intercept). The migration through the electrode is at slightly lower frequencies, producing a "diffusion-like" high frequency arc, which starts with a 45 ° angle. Migration is usually coupled with the reaction contributions, so any changes to this arc will be a combination of the resistance and migration change. With diffusion, the length of diffusion pathways in the active electrode pore structure is effectively closer to the dimensions of the pore, not the total thickness of the electrode. This is usually significantly smaller than the separator dimensions, which means that in those cases, the electrolyte-based diffusion inside active electrode pores can be neglected.

Next in line of possible changes in cell design is the controlled modifications of other transport related properties of the porous layers, besides their thicknesses. Clear examples are porosity and tortuosity parameters [27]. The porosity value ε gives us a measure of the volume fraction of pores in which electrolyte can be stored. A larger value means a more open porous layer, which results in faster transport. Tortuosity τ_g is a measure of how winding/twisted the path through the porous layer is, so it serves as a correction of the thickness value, L_p. In a highly tortuous layer with a thickness of L_p, the particle must travel a significantly longer path than L_p through the layer to reach the opposite side. The effect of both parameters is included in the effective chemical diffusion coefficient $D_{chem.eff}$ and the effective values of associated parameters, e.g. effective specific conductivity, etc. The simplest example of studying the effect of porosity and tortuosity of porous layers is by changing the separator type or even omitting it through using an insulating cell spacer or beaker type cell [18,27]. Similarly, other porous layers, such as coatings or porous electrode material can be specifically designed to vary these properties, although this usually includes complex synthesis procedures [28,29]. This cell design change is therefore slightly less useful for determination of the origin of spectra contributions, since the porosity and tortuosity parameters are harder to control or change in larger magnitudes without affecting other properties of the layer. The approach could nevertheless be useful in determination of the chemical diffusion coefficient, which can serve as an independent confirmation of the correct assignation of impedance arcs when compared to the values determined with other analyses.

Two common impedance contributions which have yet to be modified through our suggested manipulations are the solid-state diffusion in insertion-based electrodes and contact resistance. The approaches of changing the former are like the explained electrolyte solution-based diffusion ones. If we want to affect its impedance contribution and magnify it, the simplest (but not an easy) way is through changing the length of the diffusing particle paths. In this case, this means manipulating the electrode active particle size. Again, for more clear results, variation for at least a factor of 3 is preferred. For changing the contact resistance between the current collector and the active electrode particles, several tricks can be used. A current collector with an improved adhesion (e.g. primary carbon coating, silver paste, …) can be used, or impedance measurements can be conducted while the cell stack is under elevated pressure [30]. This can significantly reduce the contact resistance, pinpointing the exact origin of the impedance feature.

Another more general parameter, which can be varied with the purpose of elucidating the impedance spectra contributions, is temperature. All the processes taking place in the cell are temperature dependent, so the spectra will vary when changing this parameter. This means temperature manipulation does not simplify impedance spectra in a straightforward way. One common way of employing such an approach is through determination of activation energy, E_a, from spectra measurements at multiple temperatures. Note that this analysis requires fitting of spectra to extract resistance values, so it can only be done after impedance contributions have all been assigned to specific physical-chemical processes. The value of E_a then gives us a clue about the reaction processes, or it can also be useful to determine if the compact passive layer (though which only migration of active ion can take place), is more solid-state-like or more liquid-state-like.

3.3. Approach 3: additional electrochemical, morphological and chemical analyses

After exhausting additional electrochemical impedance spectroscopy measurements on different cell designs as explained in approach 2, it is advisable to turn to other additional cell and electrode analyses. The idea here is that external physical-chemical parameters determination, morphological, and chemical analysis can support or refute impedance spectra analysis findings. Furthermore, these analyses serve as the basis for the input parameters needed when preparing an impedance spectra model as it will be discussed in the following chapter.

In terms of chemical and morphological analyses of the cell parts, the most useful determinations are those that allow for extraction of parameters determining the impedance arc size and position. All of this helps directly in impedance arc assignation. If we start with the electrolyte portion, conductivity and viscosity measurements [21] as well as determinations of diffusion coefficient(s) [31] are useful. If we expect that the electroactive ion concentration in the electrolyte can drastically change during cell operation, determination of its concentration is also important. This is especially the case in conversion-based batteries (e.g. sulfur cathodes), where active ions start dissolving in the electrolyte after the start of cell discharge [32]. For these determinations, standard solution based analytical techniques are well suited, although contact with water or air with the solutions must be prevented to ensure the determined values are reliable for battery cell conditions.

For the determination of the porous layers' properties, measurements of their thickness, porosity, pore size, particle size, and tortuosity are useful. For the commercial separator, this is commonly supplied by the manufacturer, while it must be determined in the research laboratory for any other artificial or native porous layers and layers formed during the battery cell operation. For this purpose, scanning electron microscopy (SEM) is well suited [33–35] with special tools available which allow for transfer of samples in vacuum or argon. Morphology analysis can be upgraded even further if combined with focused ion beam - scanning electron microscopy (FIB-SEM), which enables cross-section cutting and imaging [36,37]. From these images, the information on the layer thickness, pore size and porosity as well as an estimation of tortuosity can be made. Note that the electrode usually must be washed before this morphological analysis - to remove the salt residue the electrolyte leaves on it after its removal from the cell. This must be done with care, since washing can change the layer properties if the layer is also soluble in the chosen solvent.

The morphological properties of the active porous electrode can be determined similarly as for other mentioned porous layers. For the electrode it is usually additionally important to determine its total active surface area size. This parameter dictates the size of the surface area where the charge transfer reaction can take place and consequently the R_{ct} value may be affected. Commonly, the surface area of the active material before electrode preparation is determined with gas adsorption and subsequent Brunauer–Emmett–Teller (BET) analysis [27]. One must keep in mind, though, that this surface area can drastically change after addition of the binder and electrode fabrication. More correctly, the active surface area should be determined after these manipulations. This is slightly more complex since the material is not in powder form anymore but coated on the current collector. A workaround is through mercury porosimeter or by scratching the casted material off the current collector and measuring the gas adsorption on it.

Chemical diffusion coefficient for solid state diffusion inside active Li-ion electrode particles is usually determined using intermitted titration techniques, such as GITT (galvanostatic intermitted titration test) or PITT (potentiostatic intermittent titration test), and impedance spectroscopy [38–41]. The equations used for this determination are derived from one-dimensional diffusion geometry. This assumption does not hold for real electrodes with a porous structure and particles with different size contributions. It is therefore only possible to determine the effective chemical diffusion coefficient, which is different than the solid

state diffusion coefficient. Furthermore, the lack of information about the particle active area and Li diffusion length inside the particles severely complicates the analysis [31].

Besides the morphological parameters' determination, chemical analysis can be of major help with supporting the determined mechanism of operation. What we mean by that is that the determined impedance spectra contributions should complement the knowledge on the battery operational mechanism gathered with other analytical techniques. Briefly, these can be divided into X-ray based techniques, electron and scanning probe microscopy, and spectroscopic techniques.

Among the X-ray based techniques, notable and relatively common techniques used in battery research are X-ray diffraction (XRD), which is used to study crystalline products [42–44], X-ray photoelectron spectroscopy (XPS), which is used to study the surface of selected samples and gives information on the chemical environment of selected elements on the surface, and lastly, X-ray absorption spectroscopy (XAS), which is sensitive to different oxidation states, the chemical environment, bonding type and group symmetry [45].

Microscopy covers techniques used to determine surface roughness and conductivity (atomic force microscopy, AFM) [31], the afore-mentioned morphology, particle size and distribution (SEM and FIB-SEM) [45], and atomic scale structures, crystallinity, and defects (transmission electron microscopy, TEM) [46]. Fourier transform infrared spectroscopy (IR spectroscopy), Raman spectroscopy and ultraviolet-visible light spectroscopy (UV–vis spectroscopy) are the most used approaches among spectroscopy tools [18,45]. IR and Raman provide information on chemical structure and molecular interactions and are complementary techniques. IR spectroscopy depends on a change in the dipole moment of the observed species, while Raman spectroscopy depends on a change in polarizability. UV–vis spectroscopy provides a measure of absorption of UV or visible light and in simplistic term tells us which color the measured material is. Both IR and Raman spectroscopies are mostly qualitative, while UV–vis spectroscopy can be used to quantitatively determine the concentration of light absorbing species.

3.4. Approach 4: upgrading experiments with modelling

Experiments give a direct insight into the phenomena occurring in given material. To understand the connection between different measured phenomena, we need a model, which in natural sciences is usually based on physical equations or quantitative schemes based on those equations. A good model does not only explain the existing experiments but can also provide good predictions of system's behavior under different conditions of interest. Thus, a good model may serve as an important basis for more effective planning of further experiments.

3.4.1. Levels of modelling of EIS

As in many other fields, quantitative modelling of impedance spectra can be carried out using different approaches and on various levels. First, we note that the phenomena probed with EIS mostly occur on macroscopic level which encompasses typical dimensions from several millimeters down to several nanometers and relaxation times from microseconds to hours. This means that the most reasonable level of model implementation is the so-called continuum level which typically encompasses migration of mobile ions in electric field, electrochemical interactions between electrons and ions at interfaces (solid-solid or solid-liquid) and diffusional phenomena (coupled movement of charged species due to concentration gradients in various phases found in electrodes or electrolyte).

The best-known continuum-level theory for description of battery phenomena is the concentrated solution theory (CST) for porous electrodes developed by Newman in 1960s and 1970s [47,48]. Alternatively, one can use other frameworks such as the Poisson-Nernst-Planck (PNP) diluted solution theory [49]. In any case, the impedance response of a battery cell can be calculated from such theories using at least three different approaches:

a) As a closed form (analytical) solution [50,51]
b) By transforming the equations into expressions that allow for construction of electric transmission lines involving resistors, capacitors etc. [49,52,53]
c) Using numerical approaches (usually enclosed in packages such as COMSOL Multiphysics etc.) [54–56]

Alternatively, it is sometimes possible to represent the analytical solutions as well as the transmission line modeling results as macroscopic equivalent circuits [57]. The latter approach is particularly popular due to the mathematical simplicity and wide availability of commercial software for equivalent circuit analysis. However, the simple structure of basic equivalent circuits may be deceptive and many lead to wrong analysis if the circuit has not been justified using a more rigorous physics-based treatment [58].

In the next part of this section, we will explain the main principles of all approaches whereas in the next chapter we will present typical uses of all three approaches in the field of battery impedance.

3.4.2. Analytical solutions of electrochemical impedance

Examples of analytical solutions of various basic electrochemical systems can be found in textbooks and review articles [1,3,6,8]. In the simplest case, one can imagine that active species M^{z+} with given diffusion coefficient and relatively small concentration is transported in a homogeneous electrolyte phase towards parent electrode M where it undergoes a charge transfer reaction $M^{z+} + ze^{-} = M$ (see the Fig. 6(a)). The transport step is described by a continuity equation, in the simplest case this will be the Fick's diffusion equation. The reaction kinetics can be described using the Butler-Volmer equation. As impedance spectroscopy is a low-signal technique, all the equations are linearized. Then, they are transformed from time domain into frequency domain, using either Laplace or Fourier transformation. The ratio between the transformed voltage and current signal is expressed as impedance. An example of the analytical solution for such a case is shown in the textbook edited by Macdonald and Barsoukov [3].

The impedance due to transport of species M^{z+}, i.e. Z_W, reads:

$$Z_W = \left[\frac{RT}{(zF)^2}\right]\left[\frac{L}{D_M c^0_{M^{z+}}}\right]\left[\frac{tanh\sqrt{j\omega L^2/D_M}}{\sqrt{j\omega L^2/D_M}}\right] \tag{E6}$$

where R is the gas constant, T is temperature, z is the valence number of transported active ion M^{z+} (in this case equal to the number of exchanged electrons in electrochemical reaction), F is Faraday's constant, L is the thickness of the electrolyte, D_M is the diffusion coefficient of active ion, $c^0_{M^{z+}}$ is its concentration, and ω is the angular frequency of excitation signal.

The simplest version of the linearized resistance due to charge transfer reaction, R_{ct}, is given by:

$$R_{ct} = \left[\frac{RT}{(zF)^2}\right]\left[\frac{1}{k^0_b c^0_{M^{z+}}}\right] \tag{E7}$$

where k^0_b is potential independent rate constant parameter for reduction of M^{z+} into M. Finally, the capacitance of double layer formed at the electrolyte/M interface can be written as:

$$C_{dl} = \frac{K\varepsilon_0}{L_D} \tag{E8}$$

where K is the effective dielectric constant of the electrolyte, ε_0 is the permittivity of vacuum and L_D is the effective thickness of the double layer region. The total impedance of this simplest transport-redox system, Z_{tot}, is a combination of all contributions:

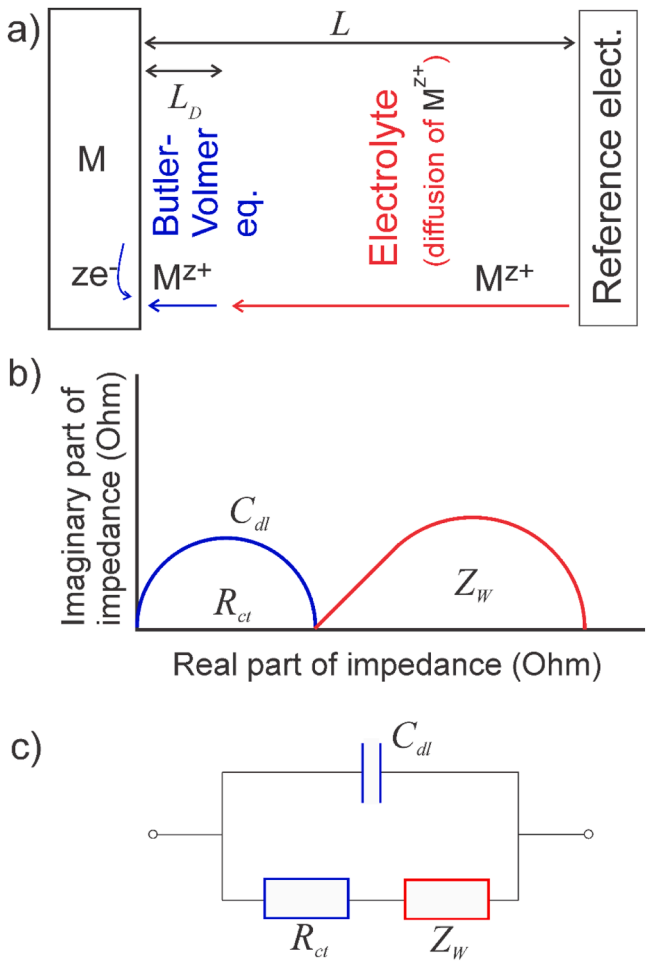

Fig. 6. (a) Schematic presentation of quite simple transport-reaction electrochemical system. (b) Impedance spectrum of system sketched in panel (a) and discussed in Eqs. (E6-E9). (c) Equivalent circuit derived from Eqs. (E6-E9). The reference electrode is positioned at the plane that divides the so-called diffusion layer close to the electrode and the bulk electrolyte where the concentration is constant.

$$Z_{tot} = \left(\frac{1}{Z_W + R_{ct}} + j\omega C_{dl}\right)^{-1} \tag{E9}$$

This solution can be plotted in complex plane as shown in Fig. 6(b).

The special benefit of having an analytical solution is that we immediately see how the impedance depends on parameter of interest. For example, one can see the inverse proportionality between R_{ct} and the rate constant (Eq. (E7)), or the inverse proportionality between double layer capacitance, C_{dl} and the thickness of double layer, L_D (Eq. (E8)). Also, we can readily embed the known equations into a simple computational program and fit our measurements with the expression for the whole impedance or for a given arc of interest. Furthermore, we can easily predict the impedance outcome if we change certain parameter, e.g. the diffusion coefficient, D_{Mz+}, or concentration, $c^0_{M^{z+}}$, of active species. Finally, we can also simplify the expression to the limiting cases of interest and get quite simple equations. For example, the "zero-frequency" limit of Warburg impedance, Z_W (Eq. (E9)) would be:

$$Z_W = \left[\frac{RT}{(zF)^2}\right]\left[\frac{L}{D_{Mz+}c^0_{Mz+}}\right] \tag{E10}$$

which is simply the resistance for transport of species M^{z+}. A further benefit of having an analytical solution is also that in most cases such solutions can be represented in a form of physics based equivalent circuit. Specifically, in our case the equivalent circuit is the well-known Randles type of circuit shown in the Fig. 6(c).

The expressions shown above are valid for the so-called flat electrodes. In many battery and other electrochemical systems (supercapacitors, fuel cells etc.) however, porous electrodes are used. This means that active material is used as small particles (of sizes on the order between about 10 nm and 10 micrometer). Particles are mixed with additives (conductive carbon, binder) which results in a porous electrode. The pores are then filled with liquid electrolyte to facilitate ionic transport to each individual active particle. Such a configuration complicates the transport-reaction mechanism significantly and requires special approaches to modeling. The best known is the Newman's approach based on the concentrate solution model developed several decades years ago [47,48] Due to elegant inclusion of concentrated electrolyte conditions, the Newman's model has remained the favorite tool for calculation of the performance (e.g. charge discharge characteristics) of various porous electrode systems. The first analytical expression for impedance of lithium battery (LIB) porous electrodes using the concentrated solution theory was demonstrated in 2007 by Sikha and White [51]. Based on this model, Huang et al. [59,60] developed a three-scale impedance model for LIB porous electrodes by considering the electrochemical reactions inside the agglomerates. Later, the approach was extended to impedance of other porous electrodes found in fuel cells, supercapacitors etc. [50].

Comparing state-of-the-art analytical solutions for impedance of porous electrodes with the corresponding typical EIS measurements, it is safe to conclude that for most cases of interest the analytical solutions represent a very good tool for analysis of impedance of battery cells with porous electrodes. The model for one porous electrode can be extended to a complete cell [61]. Based on known relationships, important criteria can be proposed to discriminate between different phenomena in a systematic and straightforward way. For example, Woillez et al. [61] recently showed which electrode configuration is appropriate for measurements of solid diffusion coefficient and where the electrolyte diffusion is overwhelming in the EIS signal. Similarly, the analytical solutions can be extended by including other physics parameters, such as effects of porosity on charge transfer resistance [62], the contact-stress effects [63], or the effect of through-plane inhomogeneities [64]. Despite significant advances in development of analytical solutions for porous electrodes, there are still many practical cases for which analytical solutions are not known. In those cases, researchers can resort to numerical or TLM approaches.

3.4.3. *Transmission line modeling of electrochemical impedance*

Transmission line modeling of porous electrodes has for many decades been based on the seminal papers by de Levie [65,66] who studied in detail the current and potential distributions in semi-infinite pore under various conditions of interest. The de Levie's approach still presents the core of most contemporary transmission line structures used in the analysis of battery impedance [67–71]. Around the year of 2000, important additional theoretical considerations regarding the application of TL modeling in various electrochemical systems were published by Bisquert [72], Jamnik et al. [52] and Barsoukov [73]. However, until the work by Lai and Ciucci [49], the TLMs for battery electrodes lacked elements that would describe diffusion in the electrolyte in the pores of porous electrolyte. Only after this inclusion, it has become possible to directly compare the Newman's model and TLM for porous electrode [53].

The physically-funded transmission line models (TMLs) start from the same set of basic transport-reaction equations as the corresponding analytical approaches discussed in previous section. However, after linearization the equations are rewritten as flux-potential relationships which already directly implies the current-voltage relationship needed for calculation of impedance [52]. After transformation of these relationships into frequency domain, one can describe all the transport-reaction space by discretized impedance elements such as

resistors and capacitors. In most practical cases electrochemical systems are considered homogeneous between the electrodes. If so, transmission lines extend in the direction from one electrode to the other.

Fig. 7 shows a transmission line that is derived for exactly the same simple system as discussed in the case of analytical solution (see Fig. 5 and the corresponding text). We can see that TLM consists of a large number (n) of resistors, R_D/n, and capacitors, C_{chem}/n, which describe the local transport/reaction phenomena between the electrodes. The meaning of the corresponding macroscopic resistor R_D for diluted systems is exactly the same as is derived analytically, namely $R_D = \left[\frac{RT}{(zF)^2}\right]\left[\frac{L}{D_M c^0_{Mz+}}\right]$ (see previous paragraph). C_{chem} is frequently termed as chemical capacitance and can also be defined for macroscopic homogeneous systems. In the case of diluted systems and for one mobile (active) species it is estimated as outlined in refs. [74,75]:

$$C_{chem} = \left[\frac{z^2F^2}{RT}\right]\left[LSc^0_{Mz+}\right] \tag{E11}$$

where S is the surface area of active metal. As we can see, all transmission line elements have an exact physical meaning and can be described using physical parameters such as diffusion coefficient, concentration, dimensions of system etc.

From the examples shown above, we can see that in the case of homogeneous systems the macroscopic values of resistors and capacitors are just sums of the local properties so in principle there is no need to use TLM (or numerical modeling). However, in the case of non-homogeneities, the relationship between the macroscopic quantities and microscopic properties may get complicated or even non-existent. In such cases the advantages of TLM become more obvious, as discussed in the Section 3.4.4 (next section).

3.4.4. Numerical modeling of electrochemical impedance

Like the other two approaches, numerical modeling also starts using the same set(s) of physical equations for transport and reactions. The equations are then discretized in space and time and solved using appropriate numerical methods [55]. The main advantage of this approach is that there are less limitations as regards the complexity of system under consideration. In this light, numerical modeling is especially important and indeed becomes indispensable (the only option) for cases that are too complex to be tackled analytically or using the TLM approach. A practical downside is that the calculation of such complex systems is computationally costly: it may take several hours or even days to calculate a single spectrum [76] whereas the analytical approach gives output within a fraction of seconds and TLM on the order of seconds up to a couple of minutes for the most demanding models. Additionally, having many parameters (usually at least about 15–20 unknown model values) can lead to ambiguous outcomes - that is one cannot discern between several explanations for a given experimental observation. This in turn generates a need for several additional sets of experiments and additional modeling which further increases the time needed for the study. This is one of the main reasons that there are few systematic coupled experimental-numerical modeling papers available in the literature.

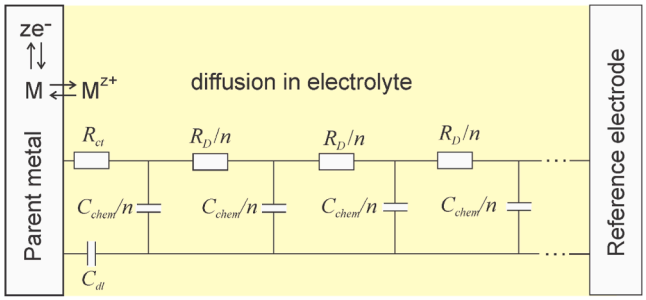

Fig. 7. Transmission line model for the same system as shown in Fig. 6. The transport in electrolyte system is discretized in n equal planes containing local elements R_D and C_{chem} the meaning of which is explained in the main text. The meaning of reaction elements R_{ct} and C_{dl} is the same as in Fig. 6. The reference electrode is positioned at the plane that divides the so-called diffusion layer close to the electrode and the bulk electrolyte where the concentration is constant.

4. Examples of impedance measurements, analyses, and modeling

4.1. Electrolyte in inert porous layers

As discussed in the Section 3, the x-axis intercept in Nyquist plot representation impedance spectra is usually called the resistive intercept and assigned to the electrolyte resistance contribution (R_{el}). In simple battery systems, the distance between the electrodes is determined by the separator properties (porosity, thickness and tortuosity). For more complex systems, with several inert porous layers present in the cell, the resistive intercept is comprised of several migration components with each of these components corresponding to a specific layer. The usual measurement equipment and setup does not, however, allow for distinction between these contributions, which are merged in a single intercept value.

The high frequency electrolyte contribution is the easiest impedance spectra feature that can be evaluated, since it is straightforwardly determined by fitting with an equivalent circuit comprising of a single resistive element (i.e. approach 1). This determination is commonly used for electrolyte conductivity determination but can be used for more complex studies as well. Any variation in the R_{el} value measured on a battery cycle by cycle is direct evidence of two drawbacks. The first one is the change of electrolyte conductivity, while the second one comes from the change in the geometrical factor of the cell (i.e. $N_M \cdot \frac{L}{S}$). Any chemical or morphological degradation of the separator or the accumulation of gas can therefore vary its value.

As discussed in Section 3.2, the electrolyte conductivity depends on the supporting salt concentration and the electrolyte viscosity. Change in its value can signal consumption of salt dissolved into the electrolyte due to parasitic chemistries that wastes Li^+ ions while forming the solid electrolyte interphases at the negative or positive electrode/electrolyte ends. Another example of change in electrolyte conductivity happens during operation of lithium-sulfur batteries. In this conversion-based battery system, sulfur is reduced during discharge to lithium polysulfides, which are well soluble in the electrolyte. This changes the electrolyte resistance depending on the state of charge of the cell. Following its value helps determine the point of highest dissolution of polysulfide species [15]. The relative change in electrolyte conductivity can also be used as a way of ranking the electrolytes by their polysulfide solubility with the highest polysulfide solubility assigned to the electrolyte exhibiting largest relative change in the value [21]

Besides the high frequency electrolyte resistance contribution, every porous layer with electrolyte filling its pores present in the cell exhibits a low frequency diffusion contribution. The later takes the form of a Warburg arc with a peak frequency dependent on the effective chemical diffusion coefficient and the diffusion path for the specific layer. This diffusion contribution is often neglected because it is hidden under other larger low frequency contributions, such as the solid-state diffusion in active particles for intercalation-based battery systems [77]. For conversion-based battery cells (sulfur or oxygen batteries), on the other hand, the feature is prominently seen and makes up a significant portion of the low frequency impedance region [15]. Likewise, Li metal anode impedance is affected by the diffusion of the active ion in the electrolyte.

Since this impedance feature is commonly superimposed with other arcs, its analysis is difficult and requires additional model experiments as well as complimentary non-electrochemical analyses (approach 4).

An example of such a study is the determination of the effect of dendritic growth on Li metal anode impedance [34], where simplified symmetrical cells were used in combination with scanning electron microscopy morphological analyses and transmission line modelling (Fig. 8).

The use of symmetrical cells enables the study of processes of a single electrode while avoiding the need for the development and incorporation of a stable reference electrode. In this case, the TLM simulations showed that the low frequency contribution was comprised of at least three different diffusion contributions – diffusion of Li^+ in separator pores, in dead Li pores, and live Li pores. The model input parameters were supported through morphological analysis of the electrodes.

4.2. Solid electrolyte interphase

The physical origin of the solid electrolyte interphase (SEI) impedance contribution is attributed to the migration of the active ion through the solid interphase formed on the battery electrode due to the electrode interaction with the electrolyte. For cathodes, this film is often termed the cathode electrolyte interphase (CEI) to distinguish it from the anode SEI. Depending on the geometry of the electrode, the contribution can either be in the form of a symmetrical arc (for a flat electrode) or a feature with a 45° angle start at high frequencies (for a porous electrode).

The most suitable approach to characterizing the interphase impedance contributions varies according to the complexness of the cell. If one wants to determine the contributions for a full cell with two different porous electrodes, an extensive study with supporting chemical and morphological characterizations as well as modelling support is needed (approach 3). This is to ensure that overlap of features, as well as the 45° angle feature shape, originating from merging of the interphase migration contribution with the transport through the electrode porous network are considered. In some cases, the CEI feature is easily separable with respect to the dominant charge transfer semi-circle [78,79]. As an example, Brutti et al. [80] studied the evolution of the EIS spectra of a $LiNi_{0.5}Mn_{1.5}O_4$ high voltage spinel upon cycling adopting an anodic voltage cut-off at 5 V vs. Li highlighting that, whereas in the fully charged and fully discharged state only a large depressed semi-circle is observed in the Nyquist plot, in the intermediate state-of-charges the two spectral features partially separate. Also, in the case of $LiNiO_2$ electrodes a better separation of the passivation film and charge transfer phenomena can be observed by EIS [78].

For simpler cell designs, such as the study of metal anode SEI on non-cycled cells, the impedance analysis is also a lot simpler. In such cases, symmetrical cells can be employed. Furthermore, the impedance spectra usually contain the resistive intercept, a large SEI arc and small lower frequency features, so the SEI arc parameters are easily extracted (approach 1). An example of such analysis is available in ref [81], where symmetrical Li metal cells' EIS spectra were measured and fit with simple equivalent circuits to determine the process of SEI growth.

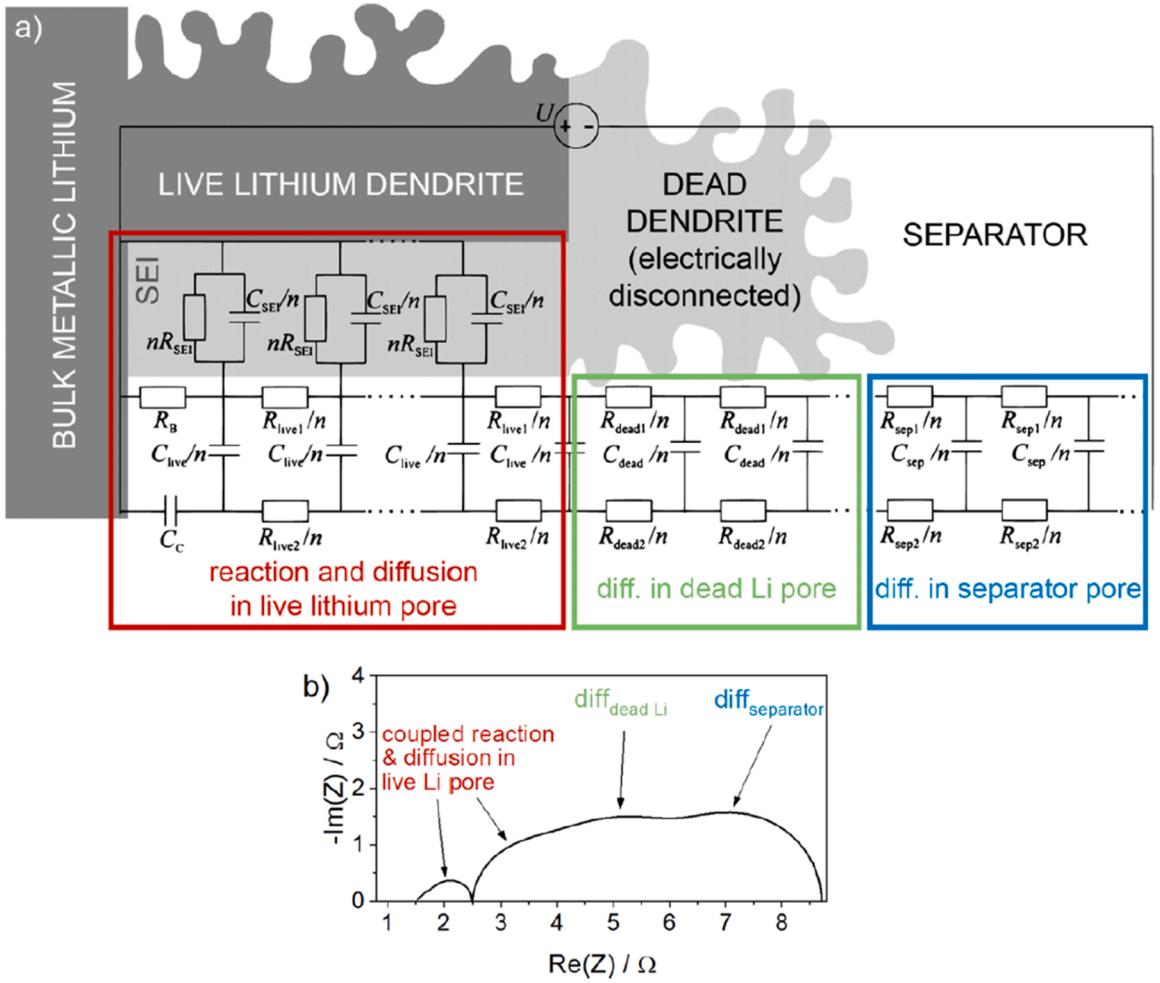

Fig. 8. Transmission line model used to describe impedance spectra of lithium electrodes with dendritic growth. Reproduced from ref. [34] with permission of American Chemical Society.

4.3. Charge transfer reaction and transport in porous electrodes

The charge transfer reaction resistance size (R_{ct}) depends on the rate constant of the reaction, the concentration of active species and the electrode's active surface area size, with the latter also affecting the double layer capacitance (C_{dl}). With that in mind, the frequency range where the feature is expected can vary widely. Furthermore, this impedance contribution is affected by the overpotential according to the Butler-Volmer relations, meaning that its size is different when measured at open circuit voltage conditions vs. under load.

For a flat electrode, the charge transfer reaction impedance constitutes a simple arc. This electrode geometry type is important in model experiments when investigating individual components and simple electrodes, however one rarely uses flat electrodes in battery cell design. It needs to be stressed that porosity is essential for many battery types, which includes the most widespread Li-ion batteries. In such, porosity arises because the electrodes consist of active powders, mixed with an electronic conductor (e.g. carbon black) and binder which forms a porous structure the pores of which are then filled with electrolyte. In such electrodes, the charge transfer reaction impedance feature is merged with the one for transport in the porous electrode in porous electrodes cells, producing an impedance feature which starts with a 45° angle at high frequencies.

Overall, charge transfer reaction impedance is therefore hard to pinpoint and requires several additional experiments to correctly attribute. An example of a study determining the charge transfer reaction impedance by model cell experiments is in ref [27]. This study employed lithium-sulfur cells simplified on multiple levels [27]. The cells were symmetrical cathode||cathode cells with the active material added in the form of a catholyte. The electrode surface size and geometry were varied between a flat glassy carbon electrode, a medium surface area carbon paper electrode and a high surface area mesoporous carbon electrode. By systematic EIS measurements (approach 2), the characteristic peak frequency of the charge transfer reaction impedance arc was determined and followed from flat electrode cells to cells with porous high surface area electrodes.

For battery systems where such simplifications are harder to execute, modelling of the porous electrode impedance response is paramount in advancing the understanding. In continuation we show several examples of porous electrode modeling using the TLM and numerical approaches.

4.3.1. Transmission line modeling of impedance of porous electrodes

Transmission line modeling of porous battery electrodes can be divided into two approaches. The first is based on the de Levie's model (Fig. 9a and b) and is particular suited for analysis of the high-frequency part (roughly above 1 Hz) of measured spectra of porous electrodes. As indicated in Fig. 9b), at higher frequencies the following processes can typically be detected: electrolyte and electronic resistance, contact impedance, migration and reaction in pores of electrode. Furthermore, one can also embed the diffusion in solid state active particles in the de Levie's model. This contribution is seen at lowest frequencies, typically on the order of 1 mHz or lower. However, we must note that at low frequencies, measurements also detect other diffusional processes such as diffusion in bulk electrolyte phase (in separator) and diffusion in the electrolyte in pores of porous electrode. Thus even if the de Levie's model does include the solid-state diffusion, it is not appropriate for accurate analysis of low-frequency properties of porous electrodes.

In cases where low frequency diffusion is also of interest, we need to use the more complete Newman's model (Fig. 9c and d). This model contains all known physical contributions due to transport and reaction

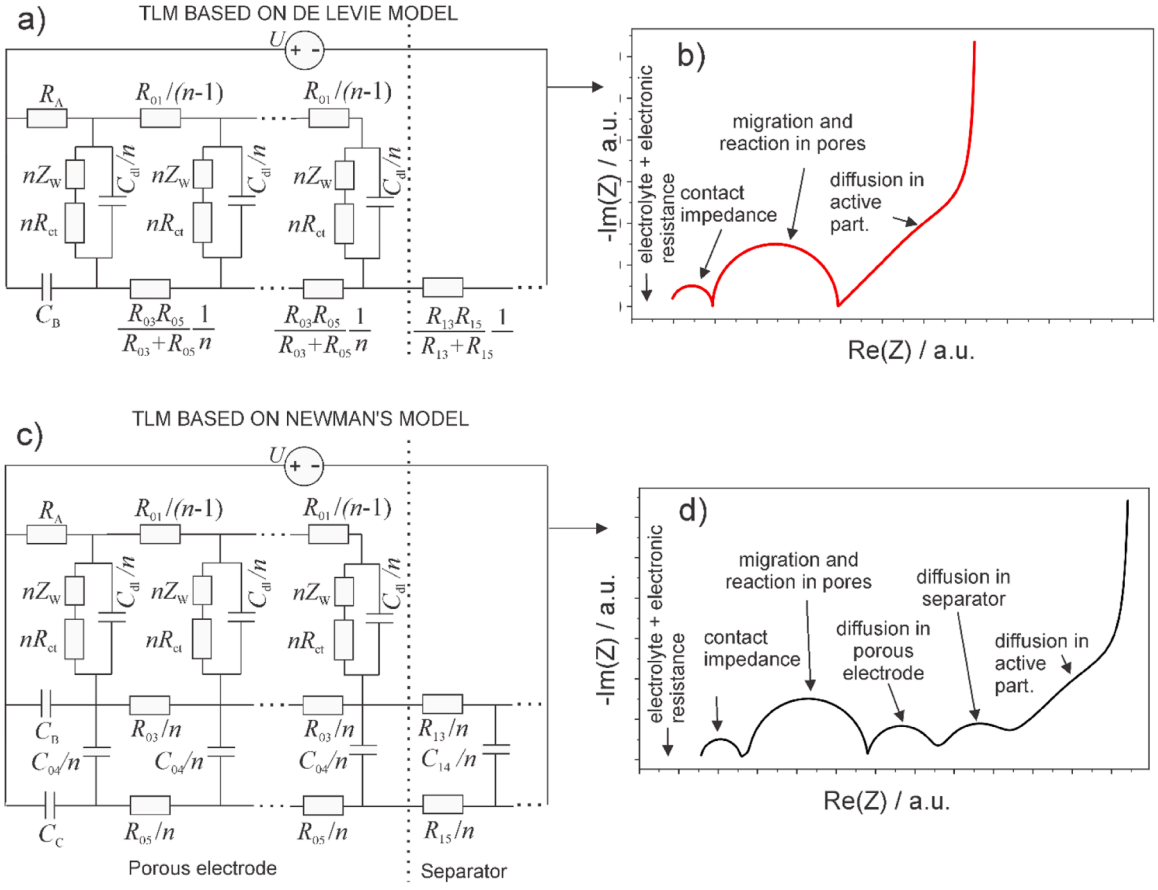

Fig. 9. a) Transmission line model and the typical EIS response based on the De Levie's approach; b) Transmission line model and the typical EIS response based on the Newman's porous electrode theory. The physical meaning of individual contributions is indicated in the complex plane graphs.

in porous electrodes on continuum level.

It is important to stress that the electrical elements (resistors, capacitors) in physics-based TLM models such as de Levie's or Newman's can be uniquely related to the actual physical quantities such as conductivity, transport number, diffusion coefficient, etc. [27,53,77]. The present authors believe that this fact is not applied frequently enough in analysis of measured impedance spectra as most authors seem to be satisfied with quantitative determination of electrical elements. However, it is also true that to calculate physical parameters from the electrical ones, we need to know the precise geometry of the porous electrode system (thickness, porosity, tortuosity, cross-section area etc.) which is frequently not available.

Furthermore, even if the geometry is known, impedance features (arcs, lines etc.) may (strongly) overlap so it is difficult to discern between different contributions. A good example of such strong overlap are all three diffusional processes highlighted in Fig. 9d): diffusion in porous electrode, diffusion in separator and diffusion in solid active particles. They all appear at low frequencies, i.e. typically in the range from 0.1 Hz to 0.1 mHz, so one typically sees a "sum" of all contributions rather than separated features sketched in the ideal response in Fig. 9d. First it needs to be noted that the strong overlap itself is not the main problem. Namely, ideal-like overlapped features can still in principle be decoupled using appropriate analytical tools. However, the measured spectra contain many deviations such as the usual measurement noise, systematic measurement errors, and in particular the so-called deviations of capacitive properties which usually appear as the so-called constant-phase elements (CPEs). All these deviations make reliable decoupling of single spectrum into individual contributions impossible. In such cases, a good practice is to make systematic experiments where the influential parameters that affect one or the other process are varied. For example, we can vary the concentration of liquid electrolyte to separate the diffusion processes in liquid and solid phases [77]. Alternatively, we could vary the size of solid active particles while maintaining the other parameters constant. Also, we may vary the electrode thickness which also has different effect on solid and liquid state diffusion [19].

In cases where we want to study very precisely one process, we may even completely change the measurement system. For example, if we want to determine as precisely as possible the transport parameters (e.g. diffusion coefficient) in solid active material, it is probably much better to use a solid-state battery configuration [57,75] instead of a porous electrode – if possible. Solid state batteries contain the active material in a form of thin film instead of porous system consisting of small particles of different sizes. The transport across thin film is much better defined, the conditions are much more homogeneous and the analysis simpler and more reliable. Thus, for analysis of measured spectra one can replace the Newman's porous electrode model (Fig. 9c and d) with much simpler equivalent circuit [57] because the only low-frequency phenomenon remains the diffusion in solid state. Also, the calculation of diffusional parameters is more reliable for planar geometry than for particulate matter because the distribution of electric field in the latter is much less clear (due to non-uniform shape and size, formation of agglomerates etc.).

Finally, we need to emphasize that in optimized cells (e.g. industrial battery cells) the special nature of porous electrode usually disappears because the transport within the pores is very fast and represents a negligible contribution to the overall impedance. In such cases the interfacial impedance (due to reaction or due to formation interfacial structures such as SEI/CEI) prevails and is seen as a separated arc. Apart from that both the electrolyte resistance and the solid-state diffusion represent the major impedance components and the system can frequently be described using a simple equivalent circuit [58]. On the other hand, due to large electrode surface area, such optimized industrial cells with very small impedances usually feature other contributions in EIS spectra such as the impedance of cables or geometrical contributions, both seen as a non-trivial addition of inductive effects [82].

4.3.2. *Numerical solutions of impedance of porous electrode*

As mentioned in the Section 3, numerical simulation of transport and reaction on the continuum level is the most straightforward way to calculate the impedance of batteries and compare the results with measurements. The main problem is usually the computation cost in solving the highly nonlinear partial differential equations which means that the simulations are comparatively slow. The latter is one of the reasons that there are few studies where researchers couple numerical analysis directly with systematic experiments to explain a given phenomenon. An example of such systematic experimental-modeling study is investigation of the effect of porosity heterogeneity on operation of porous electrodes in Li ion batteries [55,76].

As shown in Fig. 10, the authors assumed that electrode porosity can change along x-axis (across the electrode composite) due to specifics of manufacturing process, especially when preparing thicker electrodes.

The question that needs to be answered is how such heterogeneity may affect the transport properties. The authors first generated electrodes with different porosities using a previously developed stochastic method [83]. Then they calculated the electrode impedance for different cases denoted as cell-1, cell-2, cell-3 and cell-4 in Fig. 10. Importantly, to probe the ionic transport in pores as accurately as possible, the authors used the so-called blocking electrolyte, which is electrolyte without active ions, so no reaction occurred at the interface between active material and electrolyte. The EIS spectra were calculated in Comsol Multi- physics 5.4 environment using the Battery Module. The impedance was calculated at seven frequencies per decade, ranging from 1 to 10 7 Hz with 10 mV perturbation. Each simulation took approximately 15 to 30 h, depending on the input parameters (electronic conductivity of active material) and the electrode meso-structure.

The outcome of the calculations and following impedance analyses was noticeably clear: electrode heterogeneity along the thickness direction has a significant effect on the ionic impedance and capacity of the electrode. The electrode region close to the separator side has the most prominent role in ionic impedance and tortuosity factors which consequently influences the overall capacity. Therefore, to obtain the optimal electrode meso-structure with the highest performance, electrode porosity must be constructed to decrease from the separator side to the current collector side. Similar microstructure model based on numerical computational geometry have been recently reported by various authors [84–86].

5. Conclusion and perspective

Electrochemical impedance spectroscopy is a powerful and precise electrochemical method that can theoretically separate the impedance contributions of processes that take place on different time scales. However, obtaining reliable and repeatable measurement data on realistic systems requires considerable effort. For more complex electrochemical systems such as batteries, a few spectra, even if obtained through well-designed experiments, are not sufficient to decouple the various parallel phenomena and draw meaningful conclusions. Therefore, special model experiments, other complementary (electro)chemical analyzes, or modeling of impedance spectra are required. In this review, we aim to help the reader to obtain relevant data and valid conclusions by presenting different approaches for impedance spectroscopic studies. We have also presented best practices for the case of lithium batteries, while the guidelines presented are general in the sense that they can lead to reliable and valuable impedance spectroscopy experiments for most electrochemical systems.

CRediT authorship contribution statement

Sara Drvarič Talian: Writing – original draft, Validation, Funding acquisition, Conceptualization. **Sergio Brutti:** Writing – review &

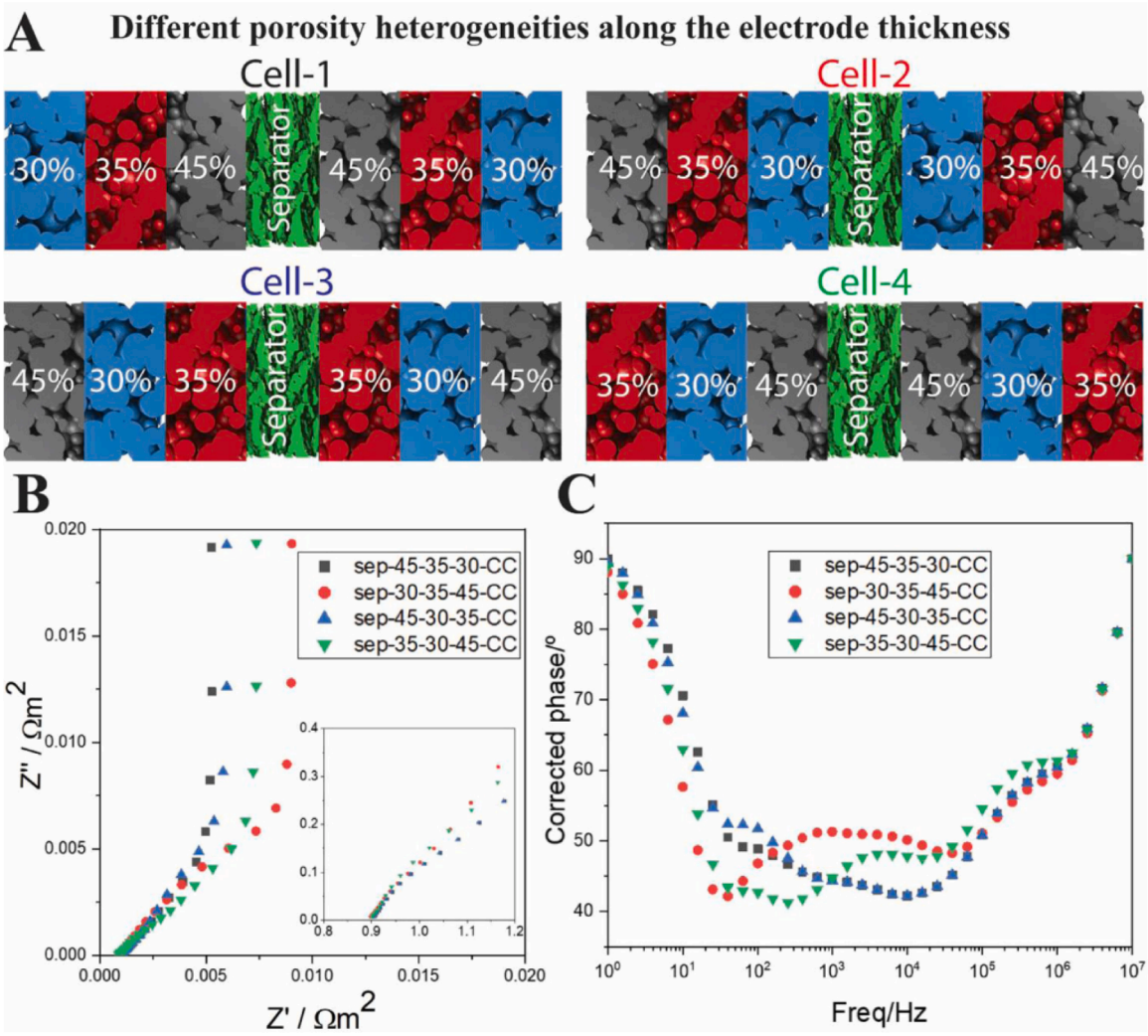

Fig. 10. A) Schematics of the different simulated symmetric cells with different porosity heterogeneities across the thickness; B) Simulated Nyquist and C) Bode plots for these symmetric cells. Reproduced from [76] with permission from Elsevier.

editing, Writing – original draft, Project administration, Funding acquisition, Conceptualization. **Maria Assunta Navarra:** Writing – original draft, Methodology, Investigation. **Jože Moškon:** Methodology, Investigation, Data curation. **Miran Gaberscek:** Writing – review & editing, Writing – original draft, Supervision, Conceptualization.

Declaration of competing interest

The authors declare that they have no known competing financial interests or personal relationships that could have appeared to influence the work reported in this paper.

Acknowledgment

Acknowledgments will be added later to preserve the anonymity of the authors at this stage of evaluation.

References

[1] D.D. Macdonald, E. Sikora, G. Engelhardt, Characterizing electrochemical systems in the frequency domain, Electrochim. Acta 43 (1998) 87–107, https://doi.org/10.1016/S0013-4686(97)00238-7.
[2] S.-M. Park, J.-S. Yoo, Electrochemical impedance spectroscopy for better electrochemical measurements, Anal. Chem. 75 (2003).
[3] E. Barsoukov, J.R. Ross Macdonald, Impedance Spectroscopy Theory, Experiment, and Applications, William Kenan, P. of Physics, Third Edition, 2018, http://www.wiley.com/go/permissions.
[4] U.v. Alpen, K. Graf, M. Hafendörfer, Data acquisition system for electrochemical applications, J. Appl. Electrochem. 8 (1978) 557–562, https://doi.org/10.1007/BF00610802.
[5] T. Dickinson, R. Whitfield, Some experimental factors which affect the analysis of impedance measurements, Electrochim. Acta 22 (1977) 385–389, https://doi.org/10.1016/0013-4686(77)85091-3.
[6] Dr. J.R.M.E. Barsoukov, Impedance Spectroscopy, John Wiley & Sons, Inc., Hoboken, NJ, USA, 2005, https://doi.org/10.1002/0471716243.
[7] S. Wang, J. Zhang, O. Gharbi, V. Vivier, M. Gao, M.E. Orazem, Electrochemical impedance spectroscopy, Nat. Rev. Method. Primer. 1 (2021) 1–21, https://doi.org/10.1038/s43586-021-00039-w, 2021 1:1.
[8] J.O. Bockris, A.K.N. Reddy, Maria. Gamboa-Aldeco, Modern Electrochemistry, 1, Ionics, Kluwer Academic, 2002.
[9] E.E. Quashie, A. Li, P. Prior, B.A. Boukamp, Distribution (function) of relaxation times, successor to complex nonlinear least squares analysis of electrochemical impedance spectroscopy? J. Phys.: Energy 2 (2020) 042001 https://doi.org/10.1088/2515-7655/ABA9E0.
[10] Y. Lu, C.Z. Zhao, J.Q. Huang, Q. Zhang, The timescale identification decoupling complicated kinetic processes in lithium batteries, Joule 6 (2022) 1172–1198, https://doi.org/10.1016/J.JOULE.2022.05.005.
[11] E. Ivers-Tiffée, A. Weber, Evaluation of electrochemical impedance spectra by the distribution of relaxation times, J. Ceram. Soc. Jpn. 125 (2017) 193–201, https://doi.org/10.2109/JCERSJ2.16267.
[12] J. Fang, W. Shen, S.H.S. Cheng, S. Ghashghaie, H.K. Shahzad, C.Y. Chung, Four-electrode symmetric setup for electrochemical impedance spectroscopy study of Lithium–Sulfur batteries, J. Power Source. 441 (2019) 227202, https://doi.org/10.1016/J.JPOWSOUR.2019.227202.

[13] Y.-C. Lu, Q. He, H.A. Gasteiger, Probing the lithium–sulfur redox reactions: a rotating-ring disk electrode study, J. Phys. Chem. C 118 (2014) 5733–5741, https://doi.org/10.1021/jp500382s.

[14] S. Solchenbach, D. Pritzl, E.J.Y. Kong, J. Landesfeind, H.A. Gasteiger, A gold micro-reference electrode for impedance and potential measurements in lithium ion batteries, J. Electrochem. Soc. 163 (2016) A2265–A2272, https://doi.org/10.1149/2.0581610JES/XML.

[15] S. Waluś, C. Barchasz, R. Bouchet, F. Alloin, Electrochemical impedance spectroscopy study of lithium–sulfur batteries: useful technique to reveal the Li/S electrochemical mechanism, Electrochim. Acta 359 (2020) 136944, https://doi.org/10.1016/J.ELECTACTA.2020.136944.

[16] B. Stiaszny, J.C. Ziegler, E.E. Krauß, J.P. Schmidt, E. Ivers-Tiffée, Electrochemical characterization and post-mortem analysis of aged $LiMn_2O_4$–$Li(Ni_{0.5}Mn_{0.3}Co_{0.2})O_2$/graphite lithium ion batteries. Part I: cycle aging, J. Power Source. 251 (2014) 439–450, https://doi.org/10.1016/J.JPOWSOUR.2013.11.080.

[17] I. Buchberger, S. Seidlmayer, A. Pokharel, M. Piana, J. Hattendorff, P. Kudejova, R. Gilles, H.A. Gasteiger, Aging analysis of graphite/$LiNi_{1/3}Mn_{1/3}Co_{1/3}O_2$ cells using XRD, PGAA, and AC impedance, J. Electrochem. Soc. 162 (2015) A2737–A2746, https://doi.org/10.1149/2.0721514JES/XML.

[18] S. Drvarič Talian, J. Moškon, R. Dominko, M. Gaberšček, Reactivity and diffusivity of Li polysulfides: a fundamental study using impedance spectroscopy, ACS. Appl. Mater. Interface. 9 (2017) 29760–29770, https://doi.org/10.1021/acsami.7b08317.

[19] J.-M. Atebamba, J. Moskon, S. Pejovnik, M. Gaberscek, On the interpretation of measured impedance spectra of insertion cathodes for lithium-ion batteries, J. Electrochem. Soc. 157 (2010) A1218, https://doi.org/10.1149/1.3489353/XML.

[20] M.P. Gomes, I. Costa, N. Pébère, J.L. Rossi, B. Tribollet, V. Vivier, On the corrosion mechanism of Mg investigated by electrochemical impedance spectroscopy, Electrochim. Acta 306 (2019) 61–70, https://doi.org/10.1016/J.ELECTACTA.2019.03.080.

[21] S. Drvarič Talian, M. Bešter-Rogač, R. Dominko, The physicochemical properties of a [DEME][TFSI] ionic liquid-based electrolyte and their influence on the performance of lithium–sulfur batteries, Electrochim. Acta 252 (2017) 147–153, https://doi.org/10.1016/J.ELECTACTA.2017.08.168.

[22] J. Landesfeind, J. Hattendorff, A. Ehrl, W.A. Wall, H.A. Gasteiger, Tortuosity determination of battery electrodes and separators by impedance spectroscopy, J. Electrochem. Soc. 163 (2016) A1373–A1387, https://doi.org/10.1149/2.1141607jes.

[23] M. Ebner, V. Wood, Tool for tortuosity estimation in lithium ion battery porous electrodes, J. Electrochem. Soc. 162 (2015) A3064–A3070, https://doi.org/10.1149/2.0111502JES/XML.

[24] J. Landesfeind, J. Hattendorff, A. Ehrl, W.A. Wall, H.A. Gasteiger, Tortuosity determination of battery electrodes and separators by impedance spectroscopy, J. Electrochem. Soc. 163 (2016) A1373–A1387, https://doi.org/10.1149/2.1141607JES/XML.

[25] N. Ogihara, Y. Itou, T. Sasaki, Y. Takeuchi, Impedance spectroscopy characterization of porous electrodes under different electrode thickness using a symmetric cell for high-performance lithium-ion batteries, J. Phys. Chem. C 119 (2015) 4612–4619, https://doi.org/10.1021/jp512564f.

[26] E. Barsoukov, J.H. Kim, J.H. Kim, C.O. Yoon, H. Lee, Kinetics of lithium intercalation into carbon anodes: in situ impedance investigation of thickness and potential dependence, Solid. State Ion. 116 (1999) 249–261, https://doi.org/10.1016/S0167-2738(98)00411-1.

[27] S. Drvarič Talian, J. Moškon, R. Dominko, M. Gaberšček, Impedance response of porous carbon cathodes in polysulfide redox system, Electrochim. Acta 302 (2019) 169–179, https://doi.org/10.1016/J.ELECTACTA.2019.02.037.

[28] S. Franger, F.Le Cras, C. Bourbon, H. Rouault, LiFePO4 synthesis routes for enhanced electrochemical performance, Electrochem. Solid-State Lett. 5 (2002) A231, https://doi.org/10.1149/1.1506962/XML.

[29] Y.-C. Chang, H.-J. Sohn, Electrochemical impedance analysis for lithium ion intercalation into graphitized carbons, J. Electrochem. Soc. 147 (2000) 50, https://doi.org/10.1149/1.1393156/XML.

[30] M. Gaberscek, J. Moskon, B. Erjavec, R. Dominko, J. Jamnik, The importance of interphase contacts in Li ion electrodes: the meaning of the high-frequency impedance arc, Electrochem. Solid-State Lett. 11 (2008) A170, https://doi.org/10.1149/1.2964220/XML.

[31] D. Renz, M. Cronau, B. Roling, Determination of lithium diffusion coefficients in single battery active material particles by using an AFM-based steady-state diffusion depolarization technique, J. Phys. Chem. C 125 (2021) 2230–2239, https://doi.org/10.1021/acs.jpcc.0c07751.

[32] Y.X. Yin, S. Xin, Y.G. Guo, L.J. Wan, Lithium–sulfur batteries: electrochemistry, materials, and prospects, Angewand. Chem. Int. Edit. 52 (2013) 13186–13200, https://doi.org/10.1002/ANIE.201304762.

[33] J. Li, J. Zhang, X. Zhang, C. Yang, N. Xu, B. Xia, Study of the storage performance of a Li-ion cell at elevated temperature, Electrochim. Acta 55 (2010) 927–934, https://doi.org/10.1016/J.ELECTACTA.2009.09.077.

[34] S. Drvarič Talian, J. Bobnar, A. Rafael Sinigoj, I. Humar, M. Gaberšček, Transmission line model for description of the impedance response of Li electrodes with dendritic growth, J. Phys. Chem. C 123 (2019) 27997–28007, https://doi.org/10.1021/acs.jpcc.9b05887.

[35] S. Drvarič Talian, J. Bobnar, J. Moškon, R. Dominko, M. Gaberšček, Effect of high concentration of polysulfides on Li stripping and deposition, Electrochim. Acta 354 (2020) 136696, https://doi.org/10.1016/J.ELECTACTA.2020.136696.

[36] S. Drvarič Talian, G. Kapun, J. Moškon, A. Vizintin, A. Randon-Vitanova, R. Dominko, M. Gaberšček, Which process limits the operation of a Li–S system? Chem. Mater. 31 (2019) 9012–9023, https://doi.org/10.1021/acs.chemmater.9b03255.

[37] T. Yoshida, M. Takahashi, S. Morikawa, C. Ihara, H. Katsukawa, T. Shiratsuchi, J. Yamaki, Degradation mechanism and life prediction of lithium-ion batteries, J. Electrochem. Soc. 153 (2006) A576, https://doi.org/10.1149/1.2162467/XML.

[38] C.J. Wen, B.A. Boukamp, R.A. Huggins, W. Weppner, Thermodynamic and mass transport properties of " LiAl ", J. Electrochem. Soc. 126 (1979) 2258–2266, https://doi.org/10.1149/1.2128939/XML.

[39] H. Gao, Q. Wu, Y. Hu, J.P. Zheng, K. Amine, Z. Chen, Revealing the rate-limiting Li-ion diffusion pathway in ultrathick electrodes for Li-ion batteries, J. Phys. Chem. Lett. 9 (2018) 5100–5104, https://doi.org/10.1021/acs.jpclett.8b02229.

[40] D.W. Dees, S. Kawauchi, D.P. Abraham, J. Prakash, Analysis of the galvanostatic intermittent titration technique (GITT) as applied to a lithium-ion porous electrode, J. Power Source. 189 (2009) 263–268, https://doi.org/10.1016/J.JPOWSOUR.2008.09.045.

[41] J. Li, X. Xiao, F. Yang, M.W. Verbrugge, Y.T. Cheng, Potentiostatic intermittent titration technique for electrodes governed by diffusion and interfacial reaction, J. Phys. Chem. C 116 (2012) 1472–1478, https://doi.org/10.1021/JP207919Q/SUPPL_FILE/JP207919Q_SI_001.PDF.

[42] A. Matasso, D. Wetz, F. Liu, The effects of internal pressure evolution on the aging of commercial Li-ion cells, J. Electrochem. Soc. 162 (2015) A92–A97, https://doi.org/10.1149/2.0611501JES/XML.

[43] P. Teichert, G.G. Eshetu, H. Jahnke, E. Figgemeier, Degradation and aging routes of Ni-rich cathode based Li-ion batteries, Batter. (Basel) 6 (2020) 8, https://doi.org/10.3390/BATTERIES6010008, 2020, Vol. 6, Page 8.

[44] N. Dupré, J.F. Martin, J. Degryse, V. Fernandez, P. Soudan, D. Guyomard, Aging of the $LiFePO_4$ positive electrode interface in electrolyte, J. Power Source. 195 (2010) 7415–7425, https://doi.org/10.1016/J.JPOWSOUR.2010.05.042.

[45] Y. Li, M. Bettge, B. Polzin, Y. Zhu, M. Balasubramanian, D.P. Abraham, Understanding long-term cycling performance of $Li_{1.2}Ni_{0.15}Mn_{0.55}Co_{0.1}O_2$ –graphite lithium-ion cells, J. Electrochem. Soc. 160 (2013) A3006–A3019, https://doi.org/10.1149/2.002305JES/XML.

[46] G. Ning, B. Haran, B.N. Popov, Capacity fade study of lithium-ion batteries cycled at high discharge rates, J. Power Source. 117 (2003) 160–169, https://doi.org/10.1016/S0378-7753(03)00029-6.

[47] J. Newman, W. Tiedemann, Porous-electrode theory with battery applications, AIChE J. 21 (1975) 25–41, https://doi.org/10.1002/AIC.690210103.

[48] J.S. Newman, C.W. Tobias, Theoretical analysis of current distribution in porous electrodes, J. Electrochem. Soc. 109 (1962) 1183, https://doi.org/10.1149/1.2425269.

[49] W. Lai, F. Ciucci, Mathematical modeling of porous battery electrodes—revisit of Newman's model, Electrochim. Acta 56 (2011) 4369–4377, https://doi.org/10.1016/J.ELECTACTA.2011.01.012.

[50] J. Huang, J. Zhang, Theory of impedance response of porous electrodes: simplifications, inhomogeneities, non-stationarities and applications, J. Electrochem. Soc. 163 (2016) A1983–A2000, https://doi.org/10.1149/2.0901609JES/XML.

[51] G. Sikha, R.E. White, Analytical expression for the impedance response of an insertion electrode cell, J. Electrochem. Soc. 154 (2007) A43, https://doi.org/10.1149/1.2372695/XML.

[52] J. Jamnik, J. Maier, Generalised equivalent circuits for mass and charge transport: chemical capacitance and its implications, Phys. Chem. Chem. Phys. 3 (2001) 1668–1678, https://doi.org/10.1039/B100180I.

[53] al - J. Mainka, W. Gao, N. He, J. Landesfeind, J. Hattendorff, A. Ehrl, Derivation of transmission line model from the concentrated solution theory (CST) for porous electrodes, J. Electrochem. Soc. 168 (2021) 070543, https://doi.org/10.1149/1945-7111/AC1314.

[54] F.M. Kindermann, A. Noel, S.V. Erhard, A. Jossen, Long-term equalization effects in Li-ion batteries due to local state of charge inhomogeneities and their impact on impedance measurements, Electrochim. Acta 185 (2015) 107–116, https://doi.org/10.1016/J.ELECTACTA.2015.10.108.

[55] A. Shodiev, E.N. Primo, M. Chouchane, T. Lombardo, A.C. Ngandjong, A. Rucci, A. A. Franco, 4D-resolved physical model for electrochemical impedance spectroscopy of $Li(Ni_{1-x-y}Mn_xCo_y)O_2$-based cathodes in symmetric cells: consequences in tortuosity calculations, J. Power Source. 454 (2020) 227871, https://doi.org/10.1016/J.JPOWSOUR.2020.227871.

[56] M. Doyle, J.P. Meyers, J. Newman, Computer simulations of the impedance response of lithium rechargeable batteries, J. Electrochem. Soc. 147 (2000) 99, https://doi.org/10.1149/1.1393162/XML.

[57] U. Westerhoff, K. Kurbach, F. Lienesch, M. Kurrat, Analysis of lithium-ion battery models based on electrochemical impedance spectroscopy, Energy Technol. 4 (2016) 1620–1630, https://doi.org/10.1002/ENTE.201600154.

[58] M. Gaberšček, Impedance spectroscopy of battery cells: theory versus experiment, Curr. Opin. Electrochem. 32 (2022) 100917, https://doi.org/10.1016/J.COELEC.2021.100917.

[59] J. Huang, Z. Li, J. Zhang, S. Song, Z. Lou, N. Wu, An analytical three-scale impedance model for porous electrode with agglomerates in lithium-ion batteries, J. Electrochem. Soc. 162 (2015) A585–A595, https://doi.org/10.1149/2.0241504JES/XML.

[60] J. Huang, H. Ge, Z. Li, J. Zhang, An agglomerate model for the impedance of secondary particle in lithium-ion battery electrode, J. Electrochem. Soc. 161 (2014) E3202–E3215, https://doi.org/10.1149/2.027408JES/XML.

[61] E. Woillez, M. Chandesris, Insight into LIB diffusion phenomena using analytical impedance models, J. Electrochem. Soc. 170 (2023) 070527, https://doi.org/10.1149/1945-7111/ACE55B.

[62] D. Gruet, B. Delobel, D. Sicsic, I.T. Lucas, V. Vivier, On the electrochemical impedance response of composite insertion electrodes – toward a better understanding of porous electrodes, Electrochim. Acta 295 (2019) 787–800, https://doi.org/10.1016/J.ELECTACTA.2018.10.115.
[63] R. Fang, Z. Li, A modeling framework of electrochemo-mechanics of lithium-ion battery: part II. Porous electrodes with contact stress effect, J. Electrochem. Soc. 169 (2022) 090515, https://doi.org/10.1149/1945-7111/AC8EE8.
[64] B. Choudhury, B. Suthar, Analytical solutions to characterize through-plane inhomogeneity of porous electrodes using electrochemical impedance spectroscopy, J. Electrochem. Soc. 170 (2023) 100535, https://doi.org/10.1149/1945-7111/ACFCDD.
[65] R. de Levie, On porous electrodes in electrolyte solutions—IV, Electrochim. Acta 9 (1964) 1231–1245, https://doi.org/10.1016/0013-4686(64)85015-5.
[66] R. de Levie, On porous electrodes in electrolyte solutions: I. Capacitance effects, Electrochim. Acta 8 (1963) 751–780, https://doi.org/10.1016/0013-4686(63)80042-0.
[67] J. Landesfeind, M. Ebner, A. Eldiven, V. Wood, H.A. Gasteiger, Tortuosity of battery electrodes: validation of impedance-derived values and critical comparison with 3D tomography, J. Electrochem. Soc. 165 (2018) A469–A476, https://doi.org/10.1149/2.0231803JES/XML.
[68] X. Ren, P.G. Pickup, Ionic and electronic conductivity of poly-(3-methylpyrrole-4-carboxylic Acid), J. Electrochem. Soc. 139 (1992) 2097–2105, https://doi.org/10.1149/1.2221185/XML.
[69] B.D. Cahan, M.L. Daroux, E.B. Yeager, Effect of physical and geometric factors on the impedance of electrochemical power sources, J. Electrochem. Soc. 136 (1989) 1585–1590, https://doi.org/10.1149/1.2096973/XML.
[70] F.C. Laman, J.A.R. Stiles, R.J. Shank, K. Brandt, Rate limiting mechanisms in lithium—molybdenum disulfide batteries, J. Power Source. 14 (1985) 201–207, https://doi.org/10.1016/0378-7753(85)88031-9.
[71] S.J. Lenhart, D.D. Macdonald, B.G. Pound, An AC impedance study of the degradation of porous nickel battery electrodes, J. Electrochem. Soc. 135 (1988) 1063–1071, https://doi.org/10.1149/1.2095875/XML.
[72] J. Bisquert, G. Garcia-Belmonte, F. Fabregat-Santiago, A. Compte, Anomalous transport effects in the impedance of porous film electrodes, Electrochem. Commun. 1 (1999) 429–435, https://doi.org/10.1016/S1388-2481(99)00084-3.
[73] E. Barsoukov, J.H. Kim, C.O. Yoon, H. Lee, Universal battery parameterization to yield a non-linear equivalent circuit valid for battery simulation at arbitrary load, J. Power Source. 83 (1999) 61–70, https://doi.org/10.1016/S0378-7753(99)00257-8.
[74] J. Moškon, M. Gaberšček, Transmission line models for evaluation of impedance response of insertion battery electrodes and cells, J. Power Source. Adv. 7 (2021) 100047, https://doi.org/10.1016/J.POWERA.2021.100047.
[75] A.E. Bumberger, C. Steinbach, J. Ring, J. Fleig, Mass and charge transport in $Li_{1-\delta}CoO_2$ thin films–a complete set of properties and its defect chemical interpretation, Chem. Mater. 34 (2022) 10548–10560, https://doi.org/10.1021/acs.chemmater.2c02614.
[76] A. Shodiev, M. Chouchane, M. Gaberscek, O. Arcelus, J. Xu, H. Oularbi, J. Yu, J. Li, M. Morcrette, A.A. Franco, Deconvoluting the benefits of porosity distribution in layered electrodes on the electrochemical performance of Li-ion batteries, Energy Storage Mater. 47 (2022) 462–471, https://doi.org/10.1016/J.ENSM.2022.01.058.
[77] J. Moškon, J. Žuntar, S.D. Talian, R. Dominko, M. Gaberšček, A powerful transmission line model for analysis of impedance of insertion battery cells: a case study on the NMC-Li system, J. Electrochem. Soc. 167 (2020) 140539, https://doi.org/10.1149/1945-7111/ABC769.
[78] Y. Zhang, C.-Y. Wang, Cycle-life characterization of automotive lithium-ion batteries with $LiNiO_2$ cathode, J. Electrochem. Soc. 156 (2009), https://doi.org/10.1149/1.3126385.
[79] D. Aurbach, B. Markovsky, A. Rodkin, E. Levi, Y.S. Cohen, H.J. Kim, M. Schmidt, On the capacity fading of $LiCoO_2$ intercalation electrodes: the effect of cycling, storage, temperature, and surface film forming additives, Electrochim. Acta 47 (2002) 4291–4306, https://doi.org/10.1016/S0013-4686(02)00417-6.
[80] S. Brutti, G. Greco, P. Reale, S. Panero, Insights about the irreversible capacity of $LiNi_{0.5}Mn_{1.5}O_4$ cathode materials in lithium batteries, Electrochim. Acta 106 (2013), https://doi.org/10.1016/j.electacta.2013.05.111.
[81] K. Lim, J. Popovic, J. Maier, Ion transport and growth behavior of solid electrolyte interphases on Li and Na with liquid electrolytes based on impedance analysis, J. Mater. Chem. a Mater. 11 (2023) 5725–5733, https://doi.org/10.1039/D2TA09189E.
[82] S. Schindler, M.A. Danzer, Influence of cell design on impedance characteristics of cylindrical lithium-ion cells: a model-based assessment from electrode to cell level, J. Energy Storage 12 (2017) 157–166, https://doi.org/10.1016/J.EST.2017.05.002.
[83] M. Duquesnoy, T. Lombardo, M. Chouchane, E.N. Primo, A.A. Franco, Accelerating battery manufacturing optimization by combining experiments. In Silico Electrodes Generation and Machine Learning, 2020, https://doi.org/10.26434/CHEMRXIV.12473501.V2.
[84] R. Xu, Y. Yang, F. Yin, P. Liu, P. Cloetens, Y. Liu, F. Lin, K. Zhao, Heterogeneous damage in Li-ion batteries: experimental analysis and theoretical modeling, J. Mech. Phys. Solid. 129 (2019) 160–183, https://doi.org/10.1016/J.JMPS.2019.05.003.
[85] S. Hein, T. Danner, D. Westhoff, B. Prifling, R. Scurtu, L. Kremer, A. Hoffmann, A. Hilger, M. Osenberg, I. Manke, M. Wohlfahrt-Mehrens, V. Schmidt, A. Latz, Influence of conductive additives and binder on the impedance of lithium-ion battery electrodes: effect of morphology, J. Electrochem. Soc. 167 (2020) 013546, https://doi.org/10.1149/1945-7111/AB6B1D.
[86] M. Mirsalehian, B. Vossoughi, J. Kaiser, S. Pischinger, 3D heterogeneous model for electrodes in lithium-ion batteries and its application to a modified continuum model, Batter. (Basel) 9 (2023) 298, https://doi.org/10.3390/BATTERIES9060298.